

# Accepted Manuscript

Discovery of potent IDO1 inhibitors derived from tryptophan using scaffold-hopping and structure-based design approaches

Yi Zou, Yan Wang, Fang Wang, Minghao Luo, Yuezhen Li, Wen Liu, Zhangjian Huang, Yihua Zhang, Wenjie Guo, Qiang Xu, Yisheng Lai



PII: S0223-5234(17)30485-3

DOI: [10.1016/j.ejmech.2017.06.039](https://doi.org/10.1016/j.ejmech.2017.06.039)

Reference: EJMECH 9534

To appear in: *European Journal of Medicinal Chemistry*

Received Date: 5 March 2017

Revised Date: 7 June 2017

Accepted Date: 22 June 2017

Please cite this article as: Y. Zou, Y. Wang, F. Wang, M. Luo, Y. Li, W. Liu, Z. Huang, Y. Zhang, W. Guo, Q. Xu, Y. Lai, Discovery of potent IDO1 inhibitors derived from tryptophan using scaffold-hopping and structure-based design approaches, *European Journal of Medicinal Chemistry* (2017), doi: 10.1016/j.ejmech.2017.06.039.

This is a PDF file of an unedited manuscript that has been accepted for publication. As a service to our customers we are providing this early version of the manuscript. The manuscript will undergo copyediting, typesetting, and review of the resulting proof before it is published in its final form. Please note that during the production process errors may be discovered which could affect the content, and all legal disclaimers that apply to the journal pertain.

## Graphical abstract

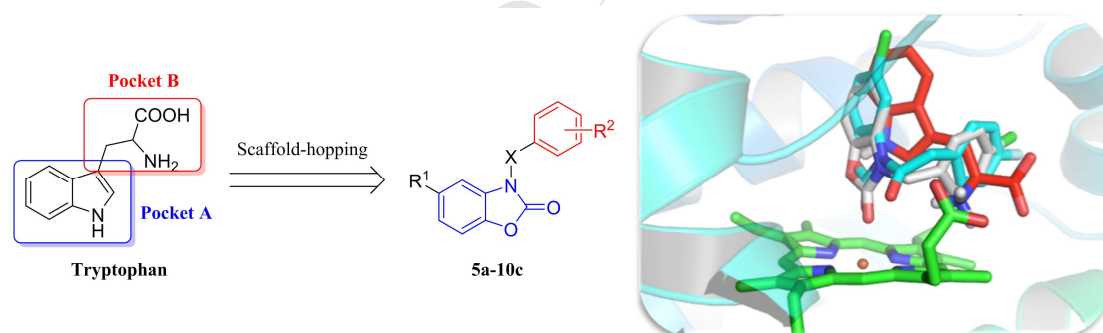
### Discovery of potent IDO1 inhibitors derived from tryptophan using scaffold-hopping and structure-based design approaches

Yi Zou <sup>a,1</sup>, Yan Wang <sup>b,1</sup>, Fang Wang <sup>a,1</sup>, Minghao Luo <sup>a</sup>, Yuezhen Li <sup>c</sup>, Wen Liu <sup>b</sup>, Zhangjian Huang <sup>a</sup>, Yihua Zhang <sup>a</sup>, Wenjie Guo <sup>b,\*\*</sup>, Qiang Xu <sup>b,\*\*</sup>, Yisheng Lai <sup>a,\*</sup>

<sup>a</sup>State Key Laboratory of Natural Medicines, Jiangsu Key Laboratory of Drug Discovery for Metabolic Diseases, Center of Drug Discovery, China Pharmaceutical University, Nanjing 210009, PR China

<sup>b</sup>State Key Laboratory of Pharmaceutical Biotechnology, School of Life Sciences, Nanjing University, Nanjing 210093, PR China

<sup>c</sup>Department of Organic Chemistry, School of Science, China Pharmaceutical University, Nanjing 211198, PR China



# Discovery of potent IDO1 inhibitors derived from tryptophan using scaffold-hopping and structure-based design approaches

Yi Zou <sup>a,1</sup>, Yan Wang <sup>b,1</sup>, Fang Wang <sup>a,1</sup>, Minghao Luo <sup>a</sup>, Yuezhen Li <sup>c</sup>, Wen Liu <sup>b</sup>,  
Zhangjian Huang <sup>a</sup>, Yihua Zhang <sup>a</sup>, Wenjie Guo <sup>b,\*\*</sup>, Qiang Xu <sup>b,\*\*</sup>, Yisheng Lai <sup>a,\*</sup>

<sup>a</sup>State Key Laboratory of Natural Medicines, Jiangsu Key Laboratory of Drug Discovery for Metabolic Diseases, Center of Drug Discovery, China Pharmaceutical University, Nanjing 210009, PR China

<sup>b</sup>State Key Laboratory of Pharmaceutical Biotechnology, School of Life Sciences, Nanjing University, Nanjing 210093, PR China

<sup>c</sup> Department of Organic Chemistry, School of Science, China Pharmaceutical University, Nanjing 211198, PR China

## Author Contributions

<sup>1</sup> Y.Z., Y.W., and F.W. contributed equally to this work.

\* Corresponding author. State Key Laboratory of Natural Medicines, Jiangsu Key Laboratory of Drug Discovery for Metabolic Diseases, Center of Drug Discovery, China Pharmaceutical University, Nanjing 210009, PR China.

\*\* Corresponding author. State Key Laboratory of Pharmaceutical Biotechnology, School of Life Sciences, Nanjing University, Nanjing 210093, PR China.

E-mail addresses: guowj@nju.edu.cn (W. Guo), molpharm@163.com (Q. Xu), yslai@cpu.edu.cn (Y. Lai).

**ABSTRACT**

Indoleamine 2,3-dioxygenase 1 (IDO1) is frequently hijacked by tumors to escape the host immune response, and the enzyme is now firmly established as an attractive target for cancer immunotherapy. To identify novel IDO1 inhibitors suitable for drug development, a scaffold-hopping strategy combined with the average electrostatic potentials calculation was utilized to design novel benzoxazolinone derivatives. Among these, compounds **7e**, **7f** and **9c** exhibited the inhibitory potency in the low micromolar range and displayed negligible level of cytotoxicity against HeLa cells. Treatment with these three compounds promoted the proliferation of T lymphocyte and led to the dramatic decrease of regulatory T cells in the B16F1 cells and naïve T cells co-culture system. Subsequent spectroscopic experiments suggested that these benzoxazolinones formed a coordinate bond with the heme iron to stabilize the complex. This study suggested that the benzoxazolinone was an interesting scaffold for discovering novel IDO1 inhibitors, and these compounds are attractive candidates for further development.

**Keywords:**

Indoleamine 2,3-dioxygenase 1; scaffold-hopping; electrostatic potentials calculation; induced fit docking; QM/MM

## 1. Introduction

Although the host immune system is able to recognize and destroy transformed cells, most malignancies can create an immunosuppressive microenvironment to evade immune destruction [1]. This can be achieved through several molecular mechanisms, including the recruitment of immunosuppressive cells, activation of immunoinhibitory checkpoint pathways, and exclusion of T cells [2]. A large body of evidence suggests that indoleamine 2,3-dioxygenase 1 (IDO1) has been proposed as a potential contributor to tumor-derived immunosuppression in the tumor microenvironment both by the depletion of tryptophan and by the accumulation of tryptophan metabolites [3].

IDO1 is an extrahepatic cytosolic heme-containing dioxygenase that catalyzes the first and rate-limiting step in the kynurenine pathway, leading to the degradation of the essential amino acid tryptophan. It is widely expressed at physiological levels in normal human tissues, including spleen, gut and lung [4]. In human cancer, in addition to being constitutively expressed by a wide variety of tumor cells via an autocrine AHR-IL-6-STAT3 signaling loop [5], IDO1 can be induced in tumor cells and the host antigen-presenting cells by proinflammatory stimuli such as interferon- $\gamma$  (IFN- $\gamma$ ) and transforming growth factor- $\beta$  (TGF- $\beta$ ) [6,7]. High expression of IDO1 by tumors can lead to the depletion of tryptophan and the accumulating high levels of kynurenine and its downstream metabolites in the tumor microenvironment, which trigger downstream signaling through GCN [8], mTOR [9] and AHR [10,11]. These events can inhibit the proliferation and function of effector T (Teff) cells [7], skew naïve CD4<sup>+</sup> T cells toward differentiation into regulatory T (Treg) cells [9], promote IDO1-expressing DCs toward an immunosuppressive phenotype [10], and thus enable tumor cells to elude the host immune response. Indeed, pharmacological inhibition of IDO1 can effectively restore antitumor immunity and suppress tumor growth in preclinical models [12], and some of IDO1 inhibitors are currently being tested in clinical trials in patients with various types of malignancies [13].

Not surprisingly, there have been many attempts to discover and develop IDO1 inhibitors in recent years. Since the design of enzyme inhibitors often begin from its substrate, many IDO1 inhibitors are tryptophan derivatives such as 1-methyltryptophan (1-MT, Fig. 1) [14]. 1-MT has two stereoisomers with different biological properties. The *L* isomer (*L*-1-MT) was the more potent IDO1 inhibitor ( $K_i = 30 \mu\text{M}$ ), while the *D* isomer (*D*-1-MT, indoximod) showed more anticancer activity in mouse tumor

models [15]. *D*-1-MT is recently in phase II clinical trials for the treatment of refractory metastatic prostate cancer (NCT01560923) and breast cancer (NCT02913430). Subsequently, a more potent inhibitor MTH-Trp with a methylthiohydantoin ring instead of the amino acidic chain of tryptophan was discovered through library screening. It was described as a competitive IDO1 inhibitor ( $K_i = 11.4 \mu\text{M}$ ) and was 20-fold more potent than 1-MT in a cell-based assay [16]. Unfortunately, in addition to IDO1, MTH-Trp also inhibits receptor-interacting serine/threonine protein kinase 1 (RIPK1), and therefore the results of the *in vitro* and *in vivo* experiments with MTH-Trp must be interpreted with caution [17,18]. In order to improve the potency of the first chemotype of IDO1 inhibitors, Donovan and co-workers undertook a screen of commercially available indole-based molecules in 2006, and found that the natural product brassinin was a moderately potent competitive inhibitor of IDO1 with a  $K_i$  value of  $97.7 \mu\text{M}$ , which bears a methylthiocarbamate moiety that replaces the  $\alpha$ -aminoacetic acid chain of tryptophan. Structural modifications of brassinin afforded the best inhibitor (**1**,  $K_i = 11.5 \mu\text{M}$ ) that was three-times more potent than 1-MT *in vitro* through the substitution of the *S*-methyl group with a naphthalene ring [19]. Then, Frédéric reported another indole series of competitive IDO1 inhibitors indol-2-yl ethanones by virtual screening, a notable example being lead compound **2** with micromolar inhibitory potency ( $\text{IC}_{50} = 65 \mu\text{M}$ ). It was characterized by an indole ring substituted in the 2-position by a 2-pyridinyl-ethanone group [20]. Then, structure and activity relationship (SAR) studies on the indol-2-yl ethanones led to the discovery compound **3** with an  $\text{IC}_{50}$  value of  $13.1 \mu\text{M}$ , and showed that an iron coordinating group on the linker was essential to retain the inhibitory activity [21].

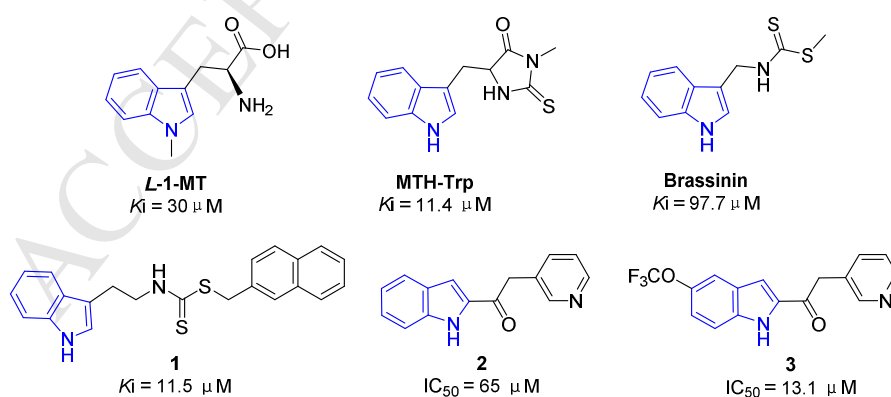


**Fig. 1.** The representative IDO1 inhibitors possessing an indole scaffold.

In addition to the above IDO1 inhibitors contained an indole fragment, many inhibitors with new structural scaffolds have been discovered by structure-based design [22], high-throughput screening

[23], and natural product derivatization [24]. Although significant progress has been made in the research mentioned above, there are currently only a few drugs in clinical trials testing IDO1 inhibition as a strategy for the treatment of cancer (*e.g.* epacadostat and GDC-0919) [25,26]. Thus, it is still an unmet need to discover novel and structurally diverse IDO1 inhibitors with characterized therapeutic utility.

In our continuous efforts to identify more potent IDO1 inhibitors, we explored here a series of novel benzo-fused five-membered heterocycles with two heteroatoms that were designed from IDO1 substrate tryptophan through a scaffold-hopping strategy (Fig. 2). Interestingly, the resulting compounds **7e**, **7f** and **9c** proved to be potent IDO1 inhibitors with inhibitory potency in the low micromolar range and displayed negligible level of cytotoxicity against HeLa cells. Subsequent experiments indicated that these compounds could promote T-cell growth, increase IFN- $\gamma$  production, and reduce the conversion of naïve T cells into Treg cells. Furthermore, the binding mode analysis of them based on induced fit docking (IFD) and quantum mechanics/molecular mechanics (QM/MM) calculation will give us a direction for further structure optimization.

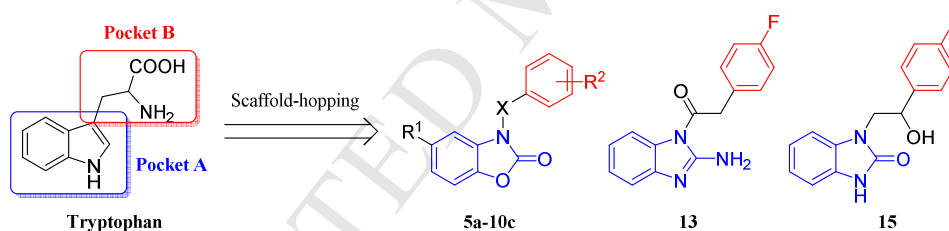


**Fig. 2.** Design strategies of the target compounds.

## 2. Results and discussion

### 2.1. Design of the target compounds

Despite the lack of IDO1 crystal structure about tryptophan binding, there is a tryptophan 2,3-dioxygenase (TDO, an enzyme functionally related to IDO1)-tryptophan complex (PDB ID: 2NW8) in protein data bank website that can be a reference for us, because key active site residues of IDO1 and TDO are conserved [27]. Through superimposing the two crystal structures (PDB ID: 4PK5 and 2NW8), we can obtain the IDO1-tryptophan complex followed by the energy minimization. As can be seen from Fig. 3, the indole ring of tryptophan is placed in pocket A of the active site, with the amino acid moiety pointing toward pocket B and positively charged amino group interacting with the heme

7-proionate group. In consideration of the importance of heme-ligand interaction and other nonbonding interactions for potent IDO1 inhibitory activity, a scaffold-hopping strategy that was the replacement of indole ring will be applied here to in-depth modification of tryptophan. First, many indole bioisosteres were utilized to perform docking experiment and the scaffolds that can directly interact with the heme iron and have indole-like shape were retained. Then, the average electrostatic potentials (ESP) calculation was used to evaluate the coordinating capability of the coordinating atom (see Supplementary data, Page S2-S9). Ultimately, benzoxazolinone whose ESP value of the coordinating oxygen atom was similar to that of 4-PI (a reported IDO1 inhibitor binding to heme iron) [28] was chosen as a starting fragment for our discovery study (Fig. 4). In addition, benzimidazolone and benzoimidazolamine moieties were also investigated for comparison.

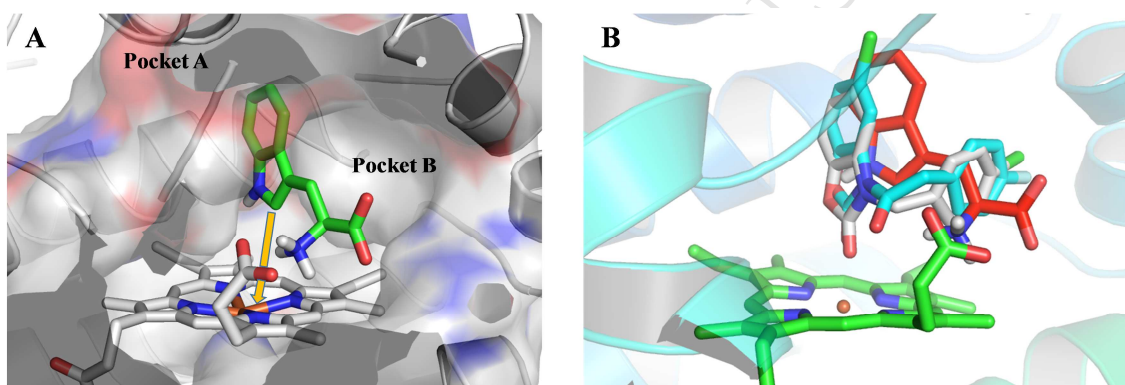


**Fig. 3.** (A) The minimized structure of IDO1-tryptophan complex. (B) Proposed binding mode of compounds **7f** (grey) and **9c** (cyan). *L*-tryptophan (red) was used as a comparison.

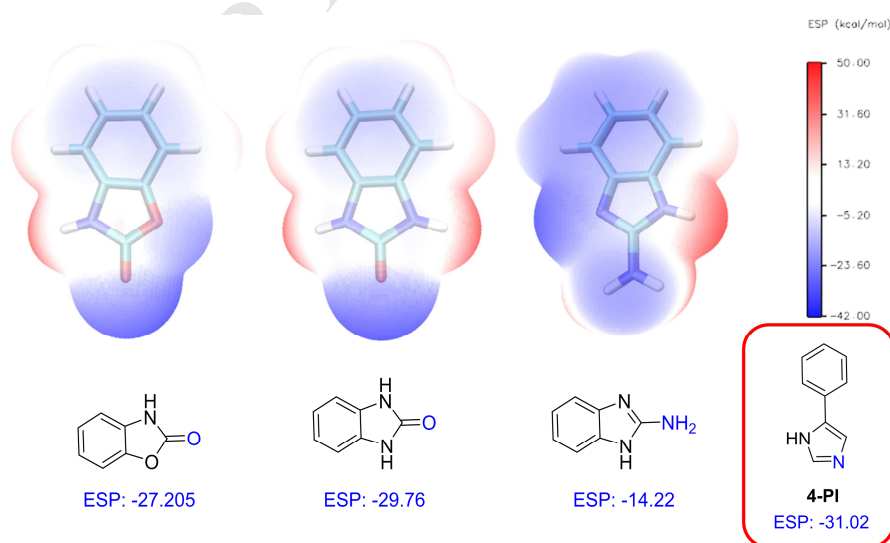
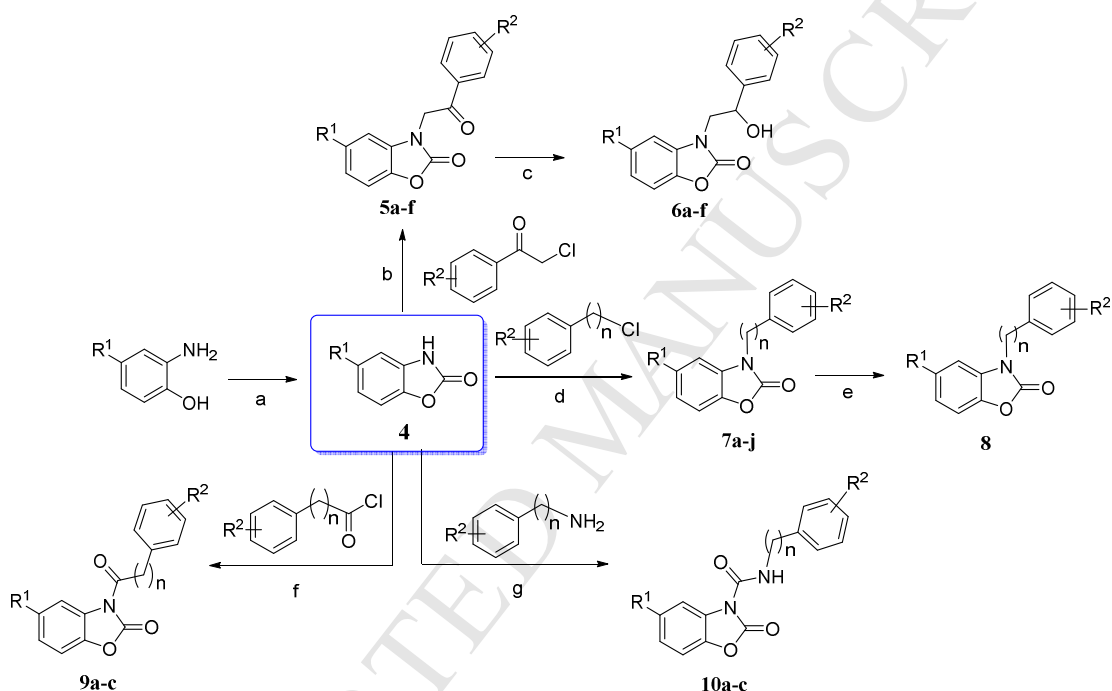


**Fig. 4.** ESP surface of three indole bioisosteres and their corresponding 2D structures. On the right side is such a plot for ESP, in which blue, white and red correspond to ESP varying from -42 to 50 kcal/mol.

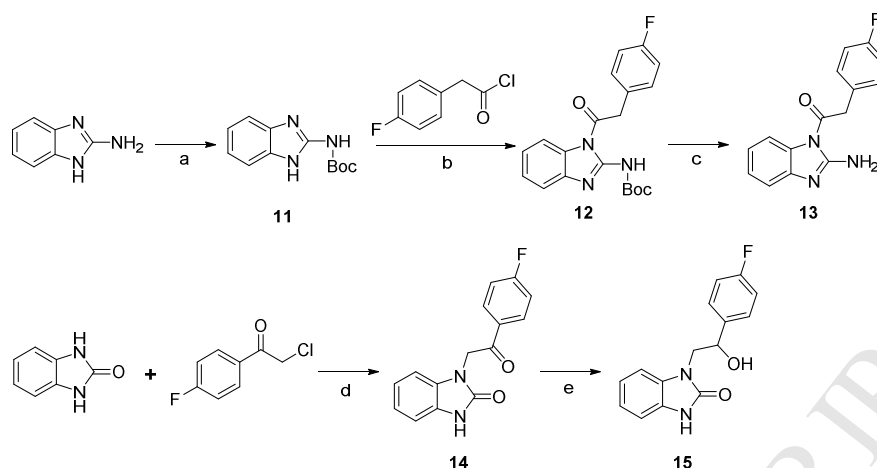
## 2.2. Synthesis of the target compounds

Synthetic route for the target compounds **5a-10c** was shown in scheme 1. The benzoxazolinone cores **4** were prepared by cyclization reaction of corresponding substituted 2-aminophenol with *N,N'*-carbonyldiimidazole (CDI), followed by substitution with various 2-chloro-1-phenylethan-1-ones, benzyl chlorides or phenyl ethyl chlorides, acyl chlorides or aromatic amines to yield **5a-5f**, **7a-7j**, **9a-9c** or **10a-10c**, respectively. In addition, **5a-5f** were reduced by sodium borohydride to give **6a-6f**, while 5-nitrobenzoxazolinone **7i** was reduced by zinc powder to yield 5-aminobenzoxazolinone **8**.



**Scheme 1.** Reagents and conditions: (a) CDI, DMF, N<sub>2</sub>, 80 °C; (b) K<sub>2</sub>CO<sub>3</sub>, DMF, 60 °C; (c) NaBH<sub>4</sub>, THF, 0 °C; (d) K<sub>2</sub>CO<sub>3</sub>, DMF, 60 °C; (e) Zn, NH<sub>4</sub>Cl, ethanol, rt; (f) TEA, THF, 70 °C; (g) Triphosgene, TEA, DCM, N<sub>2</sub>, 0 °C.

Preparation of the target compounds **13** and **15** was illustrated in scheme 2. The key intermediate **12** was obtained by acylation of the *N*-Boc protected substrate **11**, followed by cleaving the Boc-protecting group with HCl in dioxane to give the corresponding benzoimidazolamine **13**. Benzimidazolone **15** was prepared from 1,3-dihydro-2*H*-benzo[*d*]imidazol-2-one under similar conditions as that for preparation of **6**.



**Scheme 2.** Reagents and conditions: (a)  $\text{Boc}_2\text{O}$ , THF, TEA,  $60^\circ\text{C}$ ; (b) TEA, THF,  $70^\circ\text{C}$ ; (c) HCl, dioxane, r.t.; (d)  $\text{K}_2\text{CO}_3$ , DMF,  $60^\circ\text{C}$ ; (e)  $\text{NaBH}_4$ , THF,  $0^\circ\text{C}$ .

### 2.3. Inhibition of IDO1 activity

In consideration of the rapid, low-cost and valid properties of the cell-based enzymatic assay, HeLa cell line, expressing native human IDO1 induced with IFN- $\gamma$ , was used here to evaluate the inhibitory activity of these compounds against IDO1. This cellular assay, which is informative for drug development, has been widely used to investigate various IDO1 inhibitors [23c, 24b, 24c, 29], as it evaluates not only the IDO1 inhibitory effect of the compounds but also their capacity to permeate the cell and potential cytotoxicity. All synthesized compounds were assayed for their ability to inhibit tryptophan degradation and kynurenine production in the HeLa kynurenine assay, and both *L*-1-MT and GDC-0919 analog (racemic mixture of GDC-0919) were employed as the positive controls. The results were reported in Table 1.

**Table 1.** IDO1 inhibitory activity of the target compounds.

Compd.	R <sup>1</sup>	X <sup>a</sup>	R <sup>2</sup>	IC <sub>50</sub> ( $\mu\text{M}$ ) <sup>b</sup>	Compd.	R <sup>1</sup>	X <sup>a</sup>	R <sup>2</sup>	IC <sub>50</sub> ( $\mu\text{M}$ ) <sup>b</sup>
5a	H		<i>p</i> -F	53.13	7f	Cl		<i>p</i> -Cl	6.08
5b	H		<i>p</i> -Cl	38.61	7g	F		<i>m</i> -F	28.49

<b>5c</b>	H		<i>m</i> -Cl	49.25	<b>7h</b>	F		<i>p</i> -Cl	80.78
<b>5d</b>	Cl		<i>p</i> -F	20.68	<b>7i</b>	NO <sub>2</sub>		<i>m</i> -F	99.83
<b>5e</b>	Cl		<i>p</i> -Cl	24.92	<b>7j</b>	NO <sub>2</sub>		<i>p</i> -Cl	99.35
<b>5f</b>	Cl		<i>m</i> -Cl	76.58	<b>8</b>	NH <sub>2</sub>		<i>m</i> -F	> 100
<b>6a</b>	H		<i>p</i> -F	49.34	<b>9a</b>	H		<i>p</i> -F	> 100
<b>6b</b>	H		<i>p</i> -Cl	50.81	<b>9b</b>	H		H	90.49
<b>6c</b>	H		<i>m</i> -Cl	80.58	<b>9c</b>	Cl		<i>p</i> -F	6.40
<b>6d</b>	Cl		<i>p</i> -F	10.20	<b>10a</b>	H		<i>p</i> -OCH <sub>3</sub>	31.82
<b>6e</b>	Cl		<i>p</i> -Cl	62.66	<b>10b</b>	Cl		<i>m</i> -OCH <sub>3</sub>	14.56
<b>6f</b>	Cl		<i>m</i> -Cl	60.88	<b>10c</b>	Cl		<i>p</i> -OCH <sub>3</sub>	> 100
<b>7a</b>	H		H	> 100	<b>13</b>				22.73
<b>7b</b>	H		<i>m</i> -F	30.8	<b>15</b>				99.94
<b>7c</b>	H		<i>p</i> -Cl	34.96	<i>L</i> -1-MT				77.29
<b>7d</b>	Cl		H	17.91	GDC-0919 analog				0.41
<b>7e</b>	Cl		<i>m</i> -F	9.75					

<sup>a</sup> X represents the linker group connecting the benzoxazolinone core and substituted benzene ring. The left wave line represents the connection point linking with the benzoxazolinone nitrogen atom, and the right one represents the connection point linking with substituted benzene ring.

<sup>b</sup> IC<sub>50</sub> values are the mean of at least two independent assays.

The importance of the linker was first investigated. Compared with ketone (**5a-5c**) and tertiary alcohol (**6a-6c**) derivatives, the substitution with aliphatic (**7b**, **7c**) or amide group (**10a**) gave rise to the enhancement of activity to a certain extent, whereas the replacement with an ethylene moiety caused a 3-fold reduction of activity (**7a**, IC<sub>50</sub> > 100 μM). Next, we evaluated the importance of a single substitution on the phenyl ring (R<sup>2</sup> group). The *p*-chloro analogs **5b** and **6b** showed improved potency versus the analogous *m*-chloro derivatives **5c** and **6c**, respectively. According to the comparisons (**5a** versus **5b**, **6a** versus **6b**), the substitution with fluorine did not produce a remarkable

effect on IDO1 inhibition. As for the amide **10a**, we also found that the phenyl ring substituted with *p*-methoxy group did not produce any improvement of the activity ( $IC_{50} = 31.82 \mu\text{M}$ ). In addition, we studied the influence of the substituent groups at the 5-position of benzoxazolinone ( $R^1$  group). Amazingly, most of 5-chloro-substituted analogs displayed increased potency compared with the corresponding non-substituted counterpart. The two exceptions were **5f** and **6e**, which displayed slightly lower potency with an  $IC_{50}$  value of 76.58 and 62.66  $\mu\text{M}$ . Among these compounds, **7f** and **9c** exhibited high potency with  $IC_{50}$  values of 6.08 and 6.40  $\mu\text{M}$ , respectively. However, significant reduction in potency was observed for the 5-F and 5- $\text{NO}_2$  substituted analogs (**7g-j**). Compared to the 5-Cl derivative (**7e**,  $IC_{50} = 9.75 \mu\text{M}$ ), the introduction of an electron-donating amino group at 5-position (**8**,  $IC_{50} > 100 \mu\text{M}$ ) displayed significant reduction in potency, indicating that IDO1 inhibitory activity was sensitive to the electric property of the group at 5-position and 5-Cl substitution was more favorable in potency in the HeLa kynurenine assay. Finally, two different moieties, benzimidazolone and benzoimidazolamine, were also investigated through scaffold hopping. It was found that compound **13** ( $IC_{50} = 22.73 \mu\text{M}$ ) exhibited a slightly increased potency compared to **6a** (about 2-fold,  $IC_{50} = 49.34 \mu\text{M}$ ), which could be a good start point for future study. Whereas, benzimidazolone derivative **15** showed poor inhibitory effect against IDO1. These results of the SARs analysis were summarized in Fig. 5. Since the inhibition of tryptophan degradation could simply be an effect of cytotoxicity, measurement of cell viability is indispensable when reporting cellular  $IC_{50}$  values. In this study, for all compounds, cell viability was evaluated at the end of the assay in a classical MTT assay. The results of this assay indicated that most of the compounds displayed negligible level of toxicity against HeLa cells under the experimental conditions. The results of cell viability assay of **7e**, **7f**, **9c**, **13** and **15** were shown in Fig. S1.

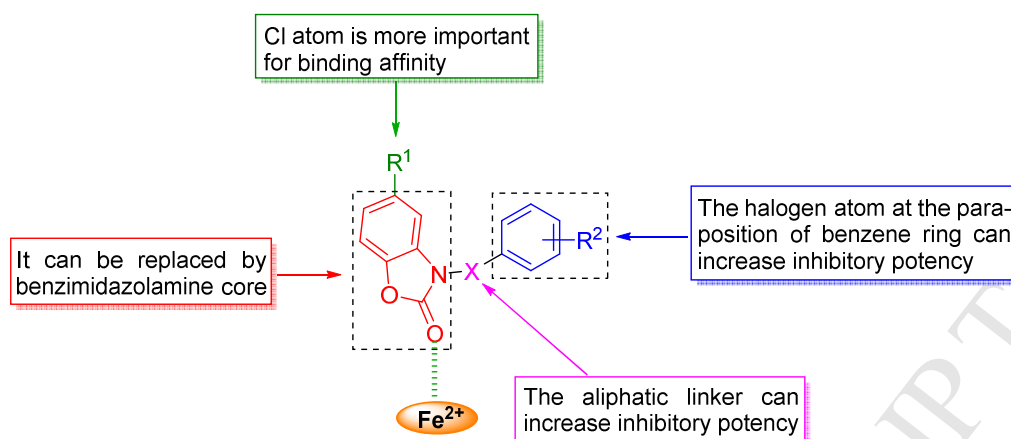


**Fig. 5.** SARs of benzoxazolinone derivatives as IDO1 inhibitors.

To this end, compounds **7e**, **7f** and **9c** were identified as better potent IDO1 inhibitors in a HeLa cell-based assay measuring IDO1-mediated tryptophan to kynurenine conversion. Further, these three compounds were turned out to be incapable of suppressing IDO1 expression through Western blot analysis, suggesting that they inhibited IDO1 enzymatic activity and not its expression in cells (Fig. 6).

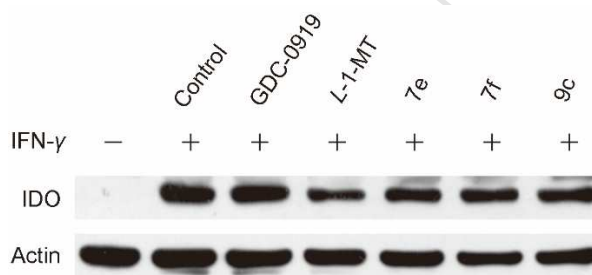


**Fig. 6.** HeLa cells were treated with IFN- $\gamma$  with or without the inhibitors at their IC<sub>50</sub> concentrations for 24 hours, and analyzed by Western blot using an anti-IDO1 antibody. GDC-0919 analog and L-1-MT were used as references.

#### 2.4. Reversal of IDO1-mediated suppression of T-cell proliferation by **7e**, **7f** and **9c**

It has been known that the resistance of IDO-expressing cells to immune rejection results from an arrest of T-cell proliferation caused by local tryptophan depletion. A proliferation assay was carried out to determine if inhibition of IDO1 activity could improve T-cell activity in the presence of cancer cells. Melanoma is known to be a highly immunogenic tumor and in many types of melanoma cells are strongly positive for IDO1 [30]. B16F1 cells, which expressed IDO1 in high level (Fig. S2), were thus used to co-culture with T cells. As shown in Fig. 7A, compounds **7e**, **7f**, **9c** and GDC-0919 analog led to a significant augmentation of T-cell activity stimulated with B16F1 cells. Especially, compound **7f** at 18  $\mu$ M displayed 52% on the rate of T-cell proliferation. These results were in conformity with the

increase of IFN- $\gamma$  levels compared with the T cells and B16F1 cells co-culture system, which can increase the growth of the neighboring T cells (Fig. 7B). Our finding was that these compounds which displayed better activity in a HeLa cell-based assay could reverse the suppression of T lymphocyte caused by IDO1 to a great extent.

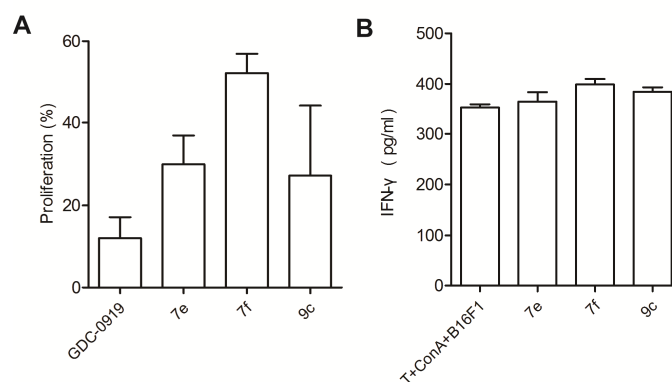


**Fig. 7.** T-cell proliferation (A) and IFN- $\gamma$  level (B) assays in the B16F1 cells-T cells co-culture system. The compounds were added to the system at the concentration of their triple IC<sub>50</sub> values from the HeLa cell-based assay ([GDC-0919]: 1.5  $\mu$ M; [7e]: 30  $\mu$ M; [7f]: 18  $\mu$ M; [9c]: 18  $\mu$ M). Each bar of the graph indicates the mean of three replicate wells with standard error of the mean.

### 2.5. Effect of 7e, 7f and 9c on Foxp3<sup>+</sup> Tregs in melanoma cells

In addition to the depletion of local tryptophan levels, IDO1 protein expressed by tumor cells leads to the accumulation of toxic tryptophan metabolites including kynurenine, anthranilic acid, 3-hydroxykynurenine, 3-hydroxyanthranilic acid and quinolinic acid [31]. They can indirectly suppress T<sub>H</sub>17 cells response by favoring differentiation of Treg cells, promoting immunoevasion and thereby favoring tumor cell growth. As Tregs are a major suppressive factor in the tumor microenvironment, we were interested to investigate whether our compounds could influence the Tregs conversion. As shown in Fig. 8, when naïve T cells co-cultured with B16F1 cells, it resulted in an approximately 2-fold increase in the number of Treg cells. Once the co-culture system treated with compounds 7e, 7f and 9c, respectively, the number of Treg cells returned to the initial level to some extent. Especially, compound 7e displayed the best effect in this test.

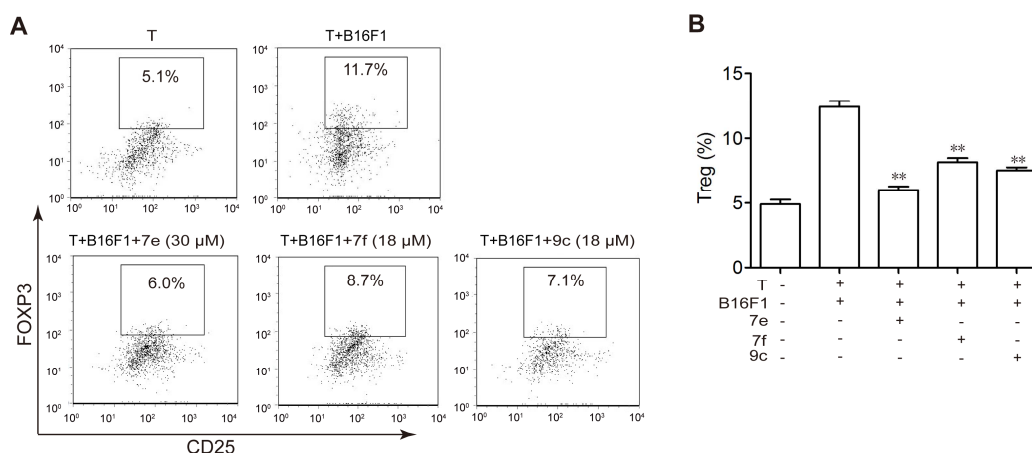


**Fig. 8.** Our IDO1 inhibitors decreased differentiation of Treg cells in the B16F1 cells-T cells co-culture system. (A) A representative plot of FACS analysis is presented.  $CD4^+CD25^+FOXP3^+$  positive cells were defined as Treg cells. (B) Average values of 3 independent experiments are shown in the graph. Error bars represent SD. \*\*  $p < 0.01$  vs T+B16F1.

## 2.6. UV-visible spectra study

Although the HeLa cell-based assay studies demonstrated the IDO1 inhibition capability of these compounds, but they failed to provide any direct evidence of ligand binding to the active site of the enzyme. Since the absorbance spectra of the heme group is highly sensitive to the local surroundings upon the ligand binding, which changes the spectral properties of the heme, UV absorption spectra of the characteristic heme peaks have been used to certify a direct binding of compounds to the iron ion in the IDO1 active site [32,33]. In this paper, we recorded the absorption spectra of ferrous-IDO1 in the absence and presence of the selected compounds. The results were shown in Fig. 9. In the absence of the compounds, the absorption spectrum of ferrous-IDO1 exhibited a Soret peak at 424 nm. Compounds **7e** and **7f** caused a decrease in the wavelength of the absorbance maxima for ferrous heme, which shifted the maxima from 424 to 418 nm. This indicated their direct binding to the  $Fe^{2+}$ -IDO1 enzyme and the reliability of ESP calculation for predicting coordinating capability.

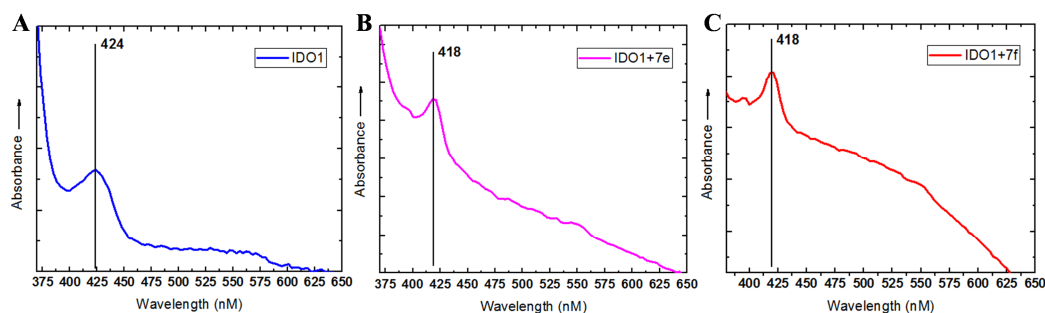


**Fig. 9.** Absorption spectra of ferrous-IDO1 (A), IDO1-compound **7e** (B) and IDO1-compound **7f** (C).

## 2.7. Molecular modeling studies

To gain insight into the molecular determinants that modulate the inhibitory activity of our compounds, molecular modeling studies were performed based on the X-ray cocrystal structure of IDO1 complex (PDB ID: 4PK5). Since the high flexibility of side chain and backbone of IDO1 protein, classical semi-flexible docking method often poses a problem for IDO1 docking, whose algorithm relies on a rigid protein structure. In addition to that, the iron-ligand interaction in the active site of IDO1 is difficult to reasonably describe by classical molecular force-field parameters [34]. All those could raise a question about the validity of predicted binding modes [35]. To overcome difficulties mentioned above, IFD method combined with QM/MM optimization was utilized in this paper. The first step was to dock the studied compound into the active site of IDO1 by the *induced fit docking* protocol in Schrödinger, which could consider the flexibility of hIDO1 protein and ligand, concurrently. In the second step, QM/MM optimization was performed by using *Qsite* to further optimize the IFD docking complex, in which a small region of the system included the full heme ring, the iron, the coordinating His residue and the inhibitor was chosen to be treated using QM calculation and the remainder of the system is treated via MM. Finally, we could reliably analyze the binding mode of the ligand in the QM/MM optimized complex (Fig. S3).

As shown in Fig. 10, the binding modes of compound **7f** presented the similar binding conformation with **9c**. The modeling of the ligand to IDO1 assumed that the benzoxazolinone core was placed deep into hydrophobic pocket A where it is perfectly situated to extend a 5-substituent chlorine atom into a small hydrophobic channel surrounded by residues Met88, Ile123, Leu124, Val125, Gly126 and Leu234. Too large (5-NO<sub>2</sub>) or too small (5-F) substituent group was not adapt to this channel and thus unfavorable for enhancing potency compared with 5-Cl group, which was in good agreement with

the experimental results. Besides the steric factor, electrical property of 5-position substituted group also influenced the binding affinity. The oxygen of the carbonyl group was found to coordinate to the heme iron with a distance of 2.06 Å for **7f**-IDO1 binding and 2.14 Å for **9c**-IDO1 binding, respectively. The replacement of 5-position by strong electron-withdrawing group such as fluorine and nitro group lowered the electron density around the coordinating oxygen atom, leading to the difficulty for the coordination bond formation. The benzene ring in the benzoxazolinone core was interacted with Tyr126 and Phe163 through  $\pi$ - $\pi$  interaction, simultaneously. The benzyl group was bent sharply at the methylene moiety and extended into the hydrophobic cavity of pocket B, interacting with Phe226 and Arg231 by  $\pi$ - $\pi$  and  $\pi$ -cation interaction, respectively. In addition to those interactions, the oxygen atom of the other carbonyl group in **9c** formed a hydrogen bond with the main chain NH group of Ala264.

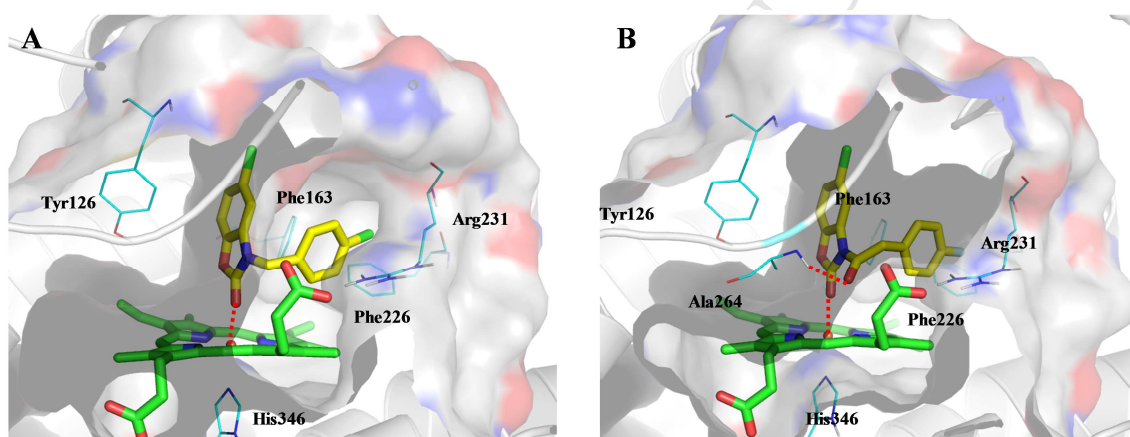


Fig. 10. QM/MM optimized structures. (A) **7f**-IDO1 complex. (B) **9c**-IDO1 complex.

### 3. Conclusion

IDO1 is a key mediator of immune escape and pathogenic inflammation in cancer and targeting the IDO1 pathway via inhibition of the IDO1 enzyme is a prime strategy for small-molecule immunomodulatory drugs in cancer therapy. A scaffold-hopping strategy combined with ESP calculation were performed in our laboratory to design novel small-molecule IDO1 inhibitors, which led to the discovery of benzoxazolinone derivatives. Subsequent modification of the linker, R<sup>1</sup> and R<sup>2</sup> substituent groups directed the identification of the most active compounds **7e**, **7f** and **9c**. Furthermore, they could promote T-cell proliferation, increase IFN- $\gamma$  production, and suppress the conversion of naïve T cells into Foxp3-expressing Treg cells. Spectroscopic experiments suggested that benzoxazolinones interacted with ferrous-IDO1 enzyme. In attempt to rationalize obtained biological

results and to improve enzyme inhibition, IFD docking and QM/MM calculation were carried out. These promising results prompt us for further development of this new class of IDO1 inhibitors.

## 4. Experimental

### 4.1. Chemistry

#### 4.1.1. General procedures

Melting points were determined on a RDCSY-I capillary apparatus and were uncorrected. All materials used were commercially available and used as supplied. HG/T2354-92 silica gel 60 F<sub>254</sub> sheets were used for analytical thin-layer chromatography (TLC). Column chromatography was performed on silica gel (200-300 mesh). <sup>1</sup>H NMR spectra were recorded on a Bruker AV-300 spectrometer. Chemical shifts ( $\delta$ ) were given in parts per million (ppm) relative to the solvent peak. *J* values are in Hz. Chemical shifts are expressed in ppm downfield from internal standard TMS. MS analyses were carried out using Shimadzu LCMS-2020 instrument. IR spectra were recorded on Shimadzu IRTracer-100 in KBr with absorptions in cm<sup>-1</sup>. All the reagents and solvents were reagent grade and were used without further purification unless otherwise specified.

#### 4.1.2. General preparation of intermediates **4**

The intermediates **4** were prepared as previously described [36] with some modification. Under the atmosphere of nitrogen, starting material aminophenol (1 equiv.) and *N,N'*-Carbonyldiimidazole (CDI) (1.2 equiv.) were mixed in DMF and stirred 80 °C for 5 h. The reaction mixture was allowed to cool to room temperature and the water was added to quench the reaction. The mixture was and extracted with ethyl acetate to afford the crude product that was purified by flash column chromatography on silica gel to yield **4a-d**.

##### 4.1.2.1. Benzo[d]oxazol-2(3H)-one (**4a**)

White solid. Yield 89%. Mp 137-139 °C. <sup>1</sup>H NMR (300 MHz, Chloroform-*d*):  $\delta$ (ppm) 9.81 (s, 1H), 8.00-6.85 (m, 4H).

##### 4.1.2.2. 5-Chlorobenzo[d]oxazol-2(3H)-one (**4b**)

White solid. Yield 87%. Mp 189-191 °C. <sup>1</sup>H NMR (300 MHz, Chloroform-*d*):  $\delta$ (ppm) 8.87 (s, 1H), 7.28 (d, *J* = 1.8 Hz, 1H), 7.13 (dp, *J* = 8.0, 2.1 Hz, 2H).

#### 4.1.2.3. 5-Fluorobenzo[d]oxazol-2(3H)-one (**4c**)

White solid. Yield 90%. Mp 174-176 °C. <sup>1</sup>H NMR (300 MHz, Chloroform-*d*):  $\delta$ (ppm) 9.60 (s, 1H), 7.13 (dd, *J* = 8.7, 4.2 Hz, 1H), 6.93-6.68 (m, 2H).

#### 4.1.2.4. 5-Nitrobenzo[d]oxazol-2(3H)-one (**4d**)

Red solid. Yield 84%. Mp 145-147 °C. <sup>1</sup>H NMR (300 MHz, Chloroform-*d*):  $\delta$ (ppm) 8.22 (d, *J* = 1.5 Hz, 1H), 8.04 (dd, *J* = 7.4, 1.6 Hz, 1H), 7.33 (d, *J* = 7.5 Hz, 1H), 6.92 (s, 1H).

#### 4.1.3. General preparation of compounds **5a-f**

A mixture of **4a** or **4b** (1 equiv.) and K<sub>2</sub>CO<sub>3</sub> (3 equiv.) in DMF was stirred at 90 °C for 1 h, then the solution was allowed to cool to 60 °C and was added different substituted 2-chloro-1-phenylethan-1-one (3 equiv.). The mixture was stirred at 60 °C for another 3 h and allowed to cool to room temperature. The saturated NH<sub>4</sub>Cl solution was added to quench the reaction. The mixture was diluted with water and was extracted with ethyl acetate to afford the crude product that was purified by flash column chromatography on silica gel to yield the target products.

##### 4.1.3.1. 3-(2-(4-Fluorophenyl)-2-oxoethyl)benzo[d]oxazol-2(3H)-one (**5a**)

White solid. Yield 85%. Mp 193-195 °C. <sup>1</sup>H NMR (300 MHz, Chloroform-*d*):  $\delta$ (ppm) 8.08 (ddd, *J* = 9.0, 5.2, 2.1 Hz, 2H), 7.39-6.96 (m, 5H), 6.85 (dq, *J* = 4.8, 3.3, 2.1 Hz, 1H), 5.22 (d, *J* = 2.0 Hz, 2H). MS (EI): *m/z* 394.1 [M+Na]<sup>+</sup>. IR (KBr): 3074, 1763, 1694, 1601, 1487, 1232 cm<sup>-1</sup>.

##### 4.1.3.2. 3-(2-(4-Chlorophenyl)-2-oxoethyl)benzo[d]oxazol-2(3H)-one (**5b**) [37]

White solid. Yield 83%. Mp 148-150 °C. <sup>1</sup>H NMR (300 MHz, Chloroform-*d*):  $\delta$ (ppm) 8.14-7.86 (m, 2H), 7.53 (d, *J* = 8.0 Hz, 2H), 7.40-7.05 (m, 3H), 6.86 (s, 1H), 5.23 (d, *J* = 3.1 Hz, 2H). MS (EI): *m/z* 288.6 [M+H]<sup>+</sup>. IR (KBr): 3065, 1763, 1691, 1587, 1487, 1246 cm<sup>-1</sup>.

##### 4.1.3.3. 3-(2-(3-Chlorophenyl)-2-oxoethyl)benzo[d]oxazol-2(3H)-one (**5c**)

White solid. Yield 85%. Mp 150-152 °C. <sup>1</sup>H NMR (300 MHz, Chloroform-*d*):  $\delta$ (ppm) 8.34-7.84 (m, 2H), 7.83-7.43 (m, 2H), 7.42-7.07 (m, 3H), 7.02-6.76 (m, 1H), 5.23 (qd, *J* = 8.4, 4.9, 4.3 Hz, 2H). MS (EI): *m/z* 288.6 [M+H]<sup>+</sup>. IR (KBr): 3071, 1722, 1683, 1601, 1512, 1229 cm<sup>-1</sup>.

##### 4.1.3.4. 5-Chloro-3-(2-(4-fluorophenyl)-2-oxoethyl)benzo[d]oxazol-2(3H)-one (**5d**)

White solid. Yield 89%. Mp 153-155 °C. <sup>1</sup>H NMR (300 MHz, Chloroform-*d*):  $\delta$ (ppm) 8.08 (d, *J* =

7.4 Hz, 2H), 7.20 (dd,  $J = 30.4, 9.8$  Hz, 4H), 6.85 (s, 1H), 5.20 (s, 2H). MS (EI):  $m/z$  306.7 [M+H]<sup>+</sup>. IR (KBr): 3076, 1771, 1690, 1599, 1487, 1232 cm<sup>-1</sup>.

#### 4.1.3.5. 5-Chloro-3-(2-(4-chlorophenyl)-2-oxoethyl)benzo[d]oxazol-2(3H)-one (**5e**) [38]

White solid. Yield 87%. Mp 167-169 °C. <sup>1</sup>H NMR (300 MHz, Chloroform-*d*):  $\delta$ (ppm) 8.05-7.93 (m, 2H), 7.60-7.50 (m, 2H), 7.24-7.12 (m, 2H), 6.85 (d,  $J = 2.0$  Hz, 1H), 5.21 (s, 2H). MS (EI):  $m/z$  323.1 [M+H]<sup>+</sup>. IR (KBr): 3067, 1772, 1719, 1589, 1485, 1246 cm<sup>-1</sup>.

#### 4.1.3.6. 5-Chloro-3-(2-(3-chlorophenyl)-2-oxoethyl)benzo[d]oxazol-2(3H)-one (**5f**)

White solid. Yield 87%. Mp 134-136 °C. <sup>1</sup>H NMR (300 MHz, Chloroform-*d*):  $\delta$ (ppm) 7.97 (d,  $J = 27.1$  Hz, 2H), 7.68 (s, 1H), 7.54 (s, 1H), 7.17 (d,  $J = 10.9$  Hz, 2H), 6.84 (s, 1H), 5.22 (s, 2H). MS (EI):  $m/z$  323.1 [M+H]<sup>+</sup>. IR (KBr): 3067, 1778, 1703, 1614, 1487, 1223 cm<sup>-1</sup>.

#### 4.1.4. General preparation of target compounds **6a-f**

To a solution one of **5a-5f** (1 equiv.) in anhydrous THF was added NaBH<sub>4</sub> (3 equiv.) at 0 °C and the mixture was stirred at that temperature for 1 h. The saturated NH<sub>4</sub>Cl solution was added to quench the reaction. The mixture was concentrated in vacuo and the residue was extracted with ethyl acetate to yield the crude product that was purified by gel chromatography to afford the target products.

#### 4.1.4.1. 3-(2-(4-Fluorophenyl)-2-hydroxyethyl)benzo[d]oxazol-2(3H)-one (**6a**)

White solid. Yield 99%. Mp 111-113 °C. <sup>1</sup>H NMR (300 MHz, Chloroform-*d*):  $\delta$ (ppm) 7.89 (s, 1H), 7.53-7.37 (m, 2H), 7.26-6.86 (m, 5H), 5.79 (t,  $J = 7.6$  Hz, 1H), 4.41 (t,  $J = 7.1$  Hz, 1H), 4.10 (t,  $J = 5.8$  Hz, 1H). MS (EI):  $m/z$  274.3 [M+H]<sup>+</sup>. IR (KBr): 3645, 3071, 1722, 1601, 1512, 1229, 1103 cm<sup>-1</sup>.

#### 4.1.4.2. 3-(2-(4-Chlorophenyl)-2-hydroxyethyl)benzo[d]oxazol-2(3H)-one (**6b**) [38]

White solid. Yield 99%. Mp 140-142 °C. <sup>1</sup>H NMR (300 MHz, Chloroform-*d*):  $\delta$ (ppm) 7.36 (q,  $J = 7.5, 6.4$  Hz, 4H), 7.15 (dq,  $J = 14.1, 6.9$  Hz, 3H), 6.99 (d,  $J = 7.0$  Hz, 1H), 5.14 (s, 1H), 3.95 (d,  $J = 10.8$  Hz, 2H), 3.06 (s, 1H). MS (EI):  $m/z$  290.7 [M+H]<sup>+</sup>. IR (KBr): 3645, 3063, 1748, 1593, 1485, 1240, 1090 cm<sup>-1</sup>.

#### 4.1.4.3. 3-(2-(3-Chlorophenyl)-2-hydroxyethyl)benzo[d]oxazol-2(3H)-one (**6c**)

White solid. Yield 99%. Mp 113-115 °C. <sup>1</sup>H NMR (300 MHz, Chloroform-*d*):  $\delta$ (ppm) 7.52-7.42 (m, 1H), 7.28 (d,  $J = 2.2$  Hz, 3H), 7.20-7.05 (m, 3H), 7.01 (dd,  $J = 7.9, 1.7$  Hz, 1H), 5.11 (dd,  $J = 8.2, 4.0$  Hz, 1H), 4.13-3.83 (m, 3H), 3.54 (s, 1H). MS (EI):  $m/z$  290.7 [M+H]<sup>+</sup>. IR (KBr): 3646, 3063, 1759,

1599, 1485, 1240, 1103 cm<sup>-1</sup>.

4.1.4.4. 5-Chloro-3-(2-(4-fluorophenyl)-2-hydroxyethyl)benzo[d]oxazol-2(3H)-one (**6d**)

White solid. Yield 99%. Mp 142-144 °C. <sup>1</sup>H NMR (300 MHz, Chloroform-*d*): δ(ppm) 7.42 (dd, *J* = 8.4, 5.3 Hz, 2H), 7.18-6.87 (m, 5H), 5.14 (dd, *J* = 8.4, 3.7 Hz, 1H), 4.17-3.79 (m, 2H), 2.94 (s, 1H). MS (EI): *m/z* 308.7 [M+H]<sup>+</sup>. IR (KBr): 3646, 3089, 1771, 1607, 1485, 1223, 1096 cm<sup>-1</sup>.

4.1.4.5. 5-Chloro-3-(2-(4-chlorophenyl)-2-hydroxyethyl)benzo[d]oxazol-2(3H)-one (**6e**) [38]

White solid. Yield 99%. Mp 127-129 °C. <sup>1</sup>H NMR (300 MHz, Chloroform-*d*): δ(ppm) 7.42-7.32 (m, 4H), 7.09 (d, *J* = 1.1 Hz, 1H), 7.08 (s, 1H), 7.03 (dd, *J* = 1.8, 0.8 Hz, 1H), 5.12 (dd, *J* = 8.3, 3.6 Hz, 1H), 3.99 (dd, *J* = 14.6, 3.6 Hz, 1H), 3.87 (dd, *J* = 14.5, 8.3 Hz, 1H), 2.97 (s, 1H). MS (EI): *m/z* 325.1 [M+H]<sup>+</sup>. IR (KBr): 3626, 3063, 1767, 1614, 1485, 1252, 1092 cm<sup>-1</sup>.

4.1.4.6. 5-Chloro-3-(2-(3-chlorophenyl)-2-hydroxyethyl)benzo[d]oxazol-2(3H)-one (**6f**)

White solid. Yield 99%. Mp 157-159 °C. <sup>1</sup>H NMR (300 MHz, Chloroform-*d*): δ(ppm) 7.45 (dq, *J* = 1.6, 0.9 Hz, 1H), 7.43-7.37 (m, 2H), 7.37-7.31 (m, 1H), 7.16-7.05 (m, 2H), 6.95 (d, *J* = 8.5 Hz, 1H), 5.74 (t, *J* = 8.3 Hz, 1H), 4.38 (t, *J* = 8.9 Hz, 1H), 4.01 (dd, *J* = 9.1, 7.9 Hz, 1H). MS (EI): *m/z* 325.1 [M+H]<sup>+</sup>. IR (KBr): 3647, 3078, 1728, 1599, 1506, 1261, 1099 cm<sup>-1</sup>.

4.1.5. General preparation of compounds **7a-j**

One of **4a-d** (1 equiv.) and K<sub>2</sub>CO<sub>3</sub> (3 equiv.) in DMF was stirred at 90 °C for 1 h, then the solution was allowed to cool to 60 °C and was added different substituted benzyl chlorides or phenyl ethyl chlorides (3 equiv.). The reaction mixture was stirred at 60 °C for another 7 h and allowed to cool to room temperature. The saturated NH<sub>4</sub>Cl solution was added to quench the reaction. The mixture was diluted with water and extracted with ethyl acetate to afford the crude product that was purified by flash column chromatography on silica gel to yield the target products.

4.1.5.1. 3-Phenethylbenzo[d]oxazol-2(3H)-one (**7a**) [39]

White solid. Yield 86%. Mp 116-118 °C. <sup>1</sup>H NMR (300 MHz, Chloroform-*d*): δ(ppm) 7.29 (d, *J* = 7.7 Hz, 3H), 7.20 (s, 3H), 7.10 (t, *J* = 5.9 Hz, 2H), 6.79 (d, *J* = 7.1 Hz, 1H), 4.06 (t, *J* = 7.4 Hz, 2H), 3.08 (t, *J* = 7.2 Hz, 2H). MS (EI): *m/z* 240.3 [M+H]<sup>+</sup>. IR (KBr): 3061, 1767, 1614, 1489, 1258 cm<sup>-1</sup>.

4.1.5.2. 3-(3-Fluorobenzyl)benzo[d]oxazol-2(3H)-one (**7b**)

White solid. Yield 88%. Mp 119-121 °C. <sup>1</sup>H NMR (300 MHz, Chloroform-*d*): δ(ppm) 7.48-7.31

(m, 2H), 7.30-6.86 (m, 6H), 5.12-4.86 (m, 2H). MS (EI):  $m/z$  244.2 [M+H]<sup>+</sup>. IR (KBr): 3042, 1757, 1589, 1487, 1252 cm<sup>-1</sup>.

#### 4.1.5.3. 3-(4-Chlorobenzyl)benzo[d]oxazol-2(3H)-one (7c)

White solid. Yield 87%. Mp 145-147 °C. <sup>1</sup>H NMR (300 MHz, Chloroform-*d*):  $\delta$ (ppm) 7.57-7.25 (m, 4H), 7.23 (s, 1H), 7.18-7.01 (m, 2H), 6.95-6.74 (m, 1H), 5.26-4.79 (m, 2H). MS (EI):  $m/z$  260.7 [M+H]<sup>+</sup>. IR (KBr): 3005, 1771, 1597, 1485, 1275 cm<sup>-1</sup>.

#### 4.1.5.4. 5-Chloro-3-phenethylbenzo[d]oxazol-2(3H)-one (7d)

White solid. Yield 88%. Mp 102-104 °C. <sup>1</sup>H NMR (300 MHz, Chloroform-*d*):  $\delta$ (ppm) 7.36-7.24 (m, 3H), 7.24-7.15 (m, 2H), 7.14-6.99 (m, 2H), 6.67 (d,  $J = 2.0$  Hz, 1H), 4.03 (t,  $J = 7.3$  Hz, 2H), 3.06 (t,  $J = 7.3$  Hz, 2H). MS (EI):  $m/z$  274.7 [M+H]<sup>+</sup>. IR (KBr): 3057, 1759, 1610, 1485, 1246 cm<sup>-1</sup>.

#### 4.1.5.5. 5-Chloro-3-(3-fluorobenzyl)benzo[d]oxazol-2(3H)-one (7e)

White solid. Yield 92%. Mp 134-136 °C. <sup>1</sup>H NMR (300 MHz, Chloroform-*d*):  $\delta$ (ppm) 7.36 (q,  $J = 11.9, 9.7$  Hz, 1H), 7.22-6.92 (m, 5H), 6.81 (d,  $J = 14.5$  Hz, 1H), 4.96 (d,  $J = 9.4$  Hz, 2H). MS (EI):  $m/z$  278.7 [M+H]<sup>+</sup>. IR (KBr): 3065, 1772, 1589, 1506, 1256 cm<sup>-1</sup>.

#### 4.1.5.6. 5-Chloro-3-(4-chlorobenzyl)benzo[d]oxazol-2(3H)-one (7f)

White solid. Yield 91%. Mp 122-124 °C. <sup>1</sup>H NMR (300 MHz, Chloroform-*d*):  $\delta$ (ppm) 7.32 (q,  $J = 8.1$  Hz, 4H), 7.23-6.97 (m, 3H), 6.90-6.73 (m, 1H), 4.95 (s, 2H). MS (EI):  $m/z$  295.1 [M+H]<sup>+</sup>. IR (KBr): 3067, 1767, 1601, 1483, 1252 cm<sup>-1</sup>.

#### 4.1.5.7. 5-Fluoro-3-(3-fluorobenzyl)benzo[d]oxazol-2(3H)-one (7g)

White solid. Yield 88%. Mp 156-158 °C. <sup>1</sup>H NMR (300 MHz, Chloroform-*d*):  $\delta$ (ppm) 7.37 (td,  $J = 8.3, 5.6$  Hz, 1H), 7.23-7.11 (m, 2H), 7.06 (dd,  $J = 10.2, 4.0$  Hz, 2H), 6.83 (td,  $J = 9.2, 2.6$  Hz, 1H), 6.59 (dd,  $J = 7.7, 2.6$  Hz, 1H), 5.00 (s, 2H). MS (EI):  $m/z$  262.1 [M+H]<sup>+</sup>. IR (KBr): 3063, 1765, 1591, 1487, 1250 cm<sup>-1</sup>.

#### 4.1.5.8. 3-(4-Chlorobenzyl)-5-fluorobenzo[d]oxazol-2(3H)-one (7h)

White solid. Yield 82%. Mp 103-105 °C. <sup>1</sup>H NMR (300 MHz, Chloroform-*d*):  $\delta$ (ppm) 7.46-7.21 (m, 4H), 7.13 (dd,  $J = 8.8, 4.2$  Hz, 1H), 6.79 (td,  $J = 9.2, 2.6$  Hz, 1H), 6.57 (dd,  $J = 7.6, 2.6$  Hz, 1H), 4.94 (s, 2H). MS (EI):  $m/z$  278.2 [M+H]<sup>+</sup>. IR (KBr): 3061, 1778, 1614, 1489, 1250 cm<sup>-1</sup>.

#### 4.1.5.9. 3-(3-Fluorobenzyl)-5-nitrobenzo[d]oxazol-2(3H)-one (**7i**)

White solid. Yield 81%. Mp 116-118 °C. <sup>1</sup>H NMR (300 MHz, Chloroform-*d*): δ(ppm) 8.42 (d, *J* = 1.8 Hz, 1H), 8.10 (dd, *J* = 7.5, 2.0 Hz, 1H), 7.40 (d, *J* = 7.5 Hz, 1H), 7.35-7.25 (m, 2H), 7.19 (dt, *J* = 8.7, 1.8 Hz, 1H), 6.97 (ddt, *J* = 8.9, 6.8, 2.3 Hz, 1H), 5.56 (d, *J* = 1.3 Hz, 2H). MS (EI): *m/z* 289.1 [M+H]<sup>+</sup>. IR (KBr): 3065, 1792, 1614, 1506, 1261 cm<sup>-1</sup>.

#### 4.1.5.10. 3-(4-Chlorobenzyl)-5-nitrobenzo[d]oxazol-2(3H)-one (**7j**)

White solid. Yield 77%. Mp 165-167 °C. <sup>1</sup>H NMR (300 MHz, Chloroform-*d*): δ(ppm) 8.14 (dd, *J* = 8.8, 2.3 Hz, 1H), 7.76 (d, *J* = 2.3 Hz, 1H), 7.48-7.29 (m, 5H), 5.05 (s, 2H). MS (EI): *m/z* 303.1 [M-H]<sup>+</sup>. IR (KBr): 3080, 1784, 1595, 1522, 1260 cm<sup>-1</sup>.

#### 4.1.6. General preparation of compounds **9a-c**

To a solution of **4a** or **4b** (1 mol equiv.) in anhydrous THF was added TEA (3 mol equiv.). The mixture was added drop wise the solution of acyl chlorides (1.1 mol equiv.) in anhydrous THF at 0 °C and stirred at 70 °C for 6 h. The water was added to quench the reaction. The mixture was extracted with ethyl acetate to afford the crude product that was purified by flash column chromatography on silica gel to yield the target products.

##### 4.1.6.1. 3-(2-(4-Fluorophenyl)acetyl)benzo[d]oxazol-2(3H)-one (**9a**)

White solid. Yield 86%. Mp 180-182 °C. <sup>1</sup>H NMR (300 MHz, DMSO-*d*<sub>6</sub>): δ(ppm) 7.98-7.89 (m, 1H), 7.50-7.41 (m, 1H), 7.41-7.28 (m, 4H), 7.24-7.14 (m, 2H), 4.41 (s, 2H). MS (EI): *m/z* 272.2 [M+H]<sup>+</sup>. IR (KBr): 3067, 1796, 1721, 1601, 1514, 1248 cm<sup>-1</sup>.

##### 4.1.6.2. 3-Benzoylbenzo[d]oxazol-2(3H)-one (**9b**) [40]

White solid. Yield 89%. Mp 185-187 °C. <sup>1</sup>H NMR (300 MHz, DMSO-*d*<sub>6</sub>): δ(ppm) 7.95-7.85 (m, 2H), 7.84-7.75 (m, 1H), 7.67 (t, *J* = 7.4 Hz, 1H), 7.53 (t, *J* = 7.6 Hz, 2H), 7.49-7.42 (m, 1H), 7.40-7.26 (m, 2H). MS (EI): *m/z* 240.2 [M+H]<sup>+</sup>. IR (KBr): 3069, 1805, 1697, 1599, 1481, 1250 cm<sup>-1</sup>.

##### 4.1.6.3. 5-Chloro-3-(2-(4-fluorophenyl)acetyl)benzo[d]oxazol-2(3H)-one (**9c**)

White solid. Yield 87%. Mp 193-195 °C. <sup>1</sup>H NMR (300 MHz, Chloroform-*d*): δ(ppm) 7.99 (d, *J* = 8.2 Hz, 2H), 7.56 (d, *J* = 8.0 Hz, 2H), 7.35-6.99 (m, 2H), 6.85 (s, 1H), 3.51 (s, 2H). MS (EI): *m/z* 306.7 [M+H]<sup>+</sup>. IR (KBr): 3063, 1755, 1715, 1611, 1485, 1246 cm<sup>-1</sup>.

#### 4.1.7. General preparation of compounds **10a-c**

To a solution of triphosgene (1 equiv.) in anhydrous dichloromethane was added **4a** or **4b** (1 equiv.) and TEA (4 equiv.) in anhydrous dichloromethane at 0 °C. Under the atmosphere of nitrogen, the mixture was stirred at room temperature for 1 h and added a mixture aromatic amines (1.5 equiv.) and TEA (1.5 equiv.) in anhydrous dichloromethane at 0 °C. The reaction was allowed to cool to room temperature and the saturated NH<sub>4</sub>Cl solution was added to quench the reaction. The mixture was diluted with water extracted with dichloromethane to afford the crude product which was purified by flash column chromatography on silica gel to yield the target products.

#### 4.1.7.1. *N*-(4-Methoxybenzyl)-2-oxobenzo[*d*]oxazole-3(2*H*)-carboxamide (**10a**)

White solid. Yield 83%. Mp 82-84 °C. <sup>1</sup>H NMR (300 MHz, DMSO-*d*<sub>6</sub>): δ(ppm) 8.56 (s, 1H), 7.89 (d, *J* = 8.0 Hz, 1H), 7.43 (s, 1H), 7.41-7.25 (m, 4H), 6.90 (d, *J* = 7.8 Hz, 2H), 4.45 (d, *J* = 4.9 Hz, 2H), 3.73 (s, 3H). MS (EI): *m/z* 299.4 [M+H]<sup>+</sup>. IR (KBr): 3266, 3009, 2951, 2870, 1761, 1722, 1612, 1514, 1275, 1260, 1034 cm<sup>-1</sup>.

#### 4.1.7.2. 5-Chloro-*N*-(3-methoxybenzyl)-2-oxobenzo[*d*]oxazole-3(2*H*)-carboxamide (**10b**)

White solid. Yield 90%. Mp 120-122 °C. <sup>1</sup>H NMR (300 MHz, Chloroform-*d*): δ(ppm) 8.37 (s, 1H), 8.15 (d, *J* = 8.2 Hz, 1H), 7.33-7.16 (m, 3H), 6.97-6.84 (m, 3H), 4.60 (d, *J* = 5.2 Hz, 2H), 3.83 (s, 3H). MS (EI): *m/z* 333.7 [M+H]<sup>+</sup>. IR (KBr): 3354, 3048, 1771, 1724, 1601, 1477, 1265, 1252, 1042 cm<sup>-1</sup>.

#### 4.1.7.3. 5-Chloro-*N*-(4-methoxyphenyl)-2-oxobenzo[*d*]oxazole-3(2*H*)-carboxamide (**10c**)

White solid. Yield 86%. Mp 162-164 °C. <sup>1</sup>H NMR (300 MHz, DMSO-*d*<sub>6</sub>): δ(ppm) 9.85 (s, 1H), 7.89 (d, *J* = 2.3 Hz, 1H), 7.53 (dd, *J* = 8.8, 2.4 Hz, 3H), 7.41-7.28 (m, 2H), 7.22-7.07 (m, 2H), 7.03-6.79 (m, 3H), 3.77 (s, 3H), 3.35 (s, 1H). MS (EI): *m/z* 319.7 [M+H]<sup>+</sup>. IR (KBr): 3291, 3036, 2957, 2866, 1784, 1734, 1609, 1477, 1246, 1182, 1034 cm<sup>-1</sup>.

#### 4.1.8. Preparation of 5-amino-3-(3-fluorobenzyl)benzo[*d*]oxazol-2(3*H*)-one (**8**)

A solution of **7i** (0.10 g, 0.37 mmol) in ethanol (10 mL) was added NH<sub>4</sub>Cl (0.19 g, 3.47 mmol) in water (2 mL) at 0 °C. After that, the mixture was added zinc powder (0.23 g, 3.47 mmol) and stirred at 0 °C for 2 h. The solution was diluted with water and extracted with ethyl acetate to afford the crude product, which was purified by flash column chromatography on silica gel to yield **8** as a white solid (0.07 g, 78%). Mp 179-181 °C. <sup>1</sup>H NMR (300 MHz, Chloroform-*d*): δ(ppm) 7.29 (d, *J* = 21.3 Hz, 2H), 7.10 (d, *J* = 7.7 Hz, 1H), 7.03-6.96 (m, 2H), 6.37 (dd, *J* = 8.5, 2.4 Hz, 1H), 6.15 (d, *J* = 2.2 Hz, 1H),

4.92 (s, 2H), 3.59 (s, 2H). MS (EI):  $m/z$  257.1 [M-H]<sup>+</sup>. IR (KBr): 3356, 3048, 1746, 1591, 1489, 1254 cm<sup>-1</sup>.

#### 4.1.9. Preparation of compound **13**

##### 4.1.9.1. *Tert-butyl (1H-benzo[d]imidazol-2-yl)carbamate (11)*

A solution of 1H-benzo[d]imidazol-2-amine (2 g, 15.02 mmol) in THF (30 mL) was added Boc<sub>2</sub>O (3.61 g, 16.52 mmol) and TEA (3.04 g, 30.04 mmol) at ambient temperature. Then, the mixture was stirred at 60 °C for 3 h. After the completion of the reaction, the mixture was cooled to room temperature and the solvent was evaporated under reduced pressure. The remained solid was washed with petroleum ether for 3 times to obtain the crude **13** (3g, 85.62%) as a white solid which will be used in the following step without any further purification.

##### 4.1.9.2. *Tert-butyl (1-(2-(4-fluorophenyl)acetyl)-1H-benzo[d]imidazol-2-yl)carbamate (12)*

This compound was prepared as a white solid following a procedure similar to that of preparation of compounds **9a-c** in 53% yield. Mp 310-312 °C. <sup>1</sup>H NMR (300 MHz, Chloroform-*d*): δ(ppm) 8.53 (s, 1H), 7.92-7.80 (m, 1H), 7.76-7.64 (dd, *J* = 7.7, 1.4 Hz, 1H), 7.41-7.21 (m, 4H), 7.11-6.99 (m, 2H), 4.04-3.88 (t, *J* = 1.0 Hz, 2H), 1.46 (s, 9H). MS (EI):  $m/z$  370.4 [M+H]<sup>+</sup>. IR (KBr): 3353, 3038, 1680, 1531, 1423, 1370 cm<sup>-1</sup>.

##### 4.1.9.3. *1-(2-Amino-1H-benzo[d]imidazol-1-yl)-2-(4-fluorophenyl)ethan-1-one (13)*

A solution of **14** (0.5g, 1.35 mmol) in dioxane (5 mL) was added HCl solution (4 M HCl in dioxane, 6.8 mL) dropwise at 0 °C. After the reaction was stirred at room temperature for 2 h, the white solid was filtered and washed with dioxane for 3 times to obtain hydrochloride, followed by the dissociation to give the free amine **15** as a white solid (0.26 g, 71.33%). Mp 237-239 °C. <sup>1</sup>H NMR (300 MHz, Chloroform-*d*): δ(ppm) 7.84-7.69 (m, 2H), 7.36-7.22 (m, 4H), 7.14-7.02 (m, 2H), 6.15-6.08 (d, *J* = 5.9 Hz, 1H), 6.06-6.00 (d, *J* = 5.9 Hz, 1H), 4.03-3.93 (t, *J* = 1.0 Hz, 2H). MS (EI):  $m/z$  270.2 [M+H]<sup>+</sup>. IR (KBr): 3356, 3148, 3048, 1646, 1591, 1419 cm<sup>-1</sup>.

#### 4.1.10. Preparation of compound **15**

##### 4.1.10.1. *1-(2-(4-Fluorophenyl)-2-oxoethyl)-1,3-dihydro-2H-benzo[d]imidazol-2-one (14)*

This compound was prepared as a white solid following a procedure similar to that of preparation of compounds **5a-f** in 78% yield. Mp 280-282 °C. <sup>1</sup>H NMR (300 MHz, Chloroform-*d*): δ(ppm)

8.22-8.03 (m, 2H), 7.43-7.31 (dd,  $J = 7.9, 1.5$  Hz, 1H), 7.26-7.14 (m, 3H), 7.12-7.06 (td,  $J = 7.6, 1.5$  Hz, 1H), 7.05-6.97 (td,  $J = 7.6, 1.5$  Hz, 1H), 5.61 (s, 2H). MS (ED):  $m/z$  273.3  $[M+H]^+$ . IR (KBr): 3323, 3018, 1687, 1520, 1439  $\text{cm}^{-1}$ .

#### 4.1.10.2. 1-(2-(4-Fluorophenyl)-2-hydroxyethyl)-1,3-dihydro-2H-benzo[d]imidazol-2-one (**15**)

This compound was prepared as a white solid following a procedure similar to that of preparation of compounds **6a-f** in 73% yield. Mp 276-278 °C.  $^1\text{H}$  NMR (300 MHz, Chloroform-*d*):  $\delta$ (ppm) 7.49-7.43 (m, 2H), 7.39-7.35 (m, 1H), 7.13-7.07 (m, 3H), 7.06-7.01 (td,  $J = 7.6, 1.5$  Hz, 1H), 7.00-6.96 (dd,  $J = 7.8, 1.5$  Hz, 1H), 5.25-5.17 (d,  $J = 6.4$  Hz, 1H), 5.14-5.07 (m, 1H), 4.38-4.27 (d,  $J = 4.9$  Hz, 2H). MS (EI):  $m/z$  273.3  $[M+H]^+$ . IR (KBr): 3570, 3343, 3028, 1670, 1521, 1449  $\text{cm}^{-1}$ .

## 4.2. Biology

### 4.2.1. HeLa cell-based enzyme assays

HeLa cells were seeded in 96-well culture plates at a density of  $5 \times 10^3$  per well. On the next day, human IFN- $\gamma$  (100 ng/mL) and compounds in a total volume of 200  $\mu\text{L}$  culture medium containing 15  $\mu\text{g}/\text{mL}$  of *L*-tryptophan were added to the cells. After incubation for 24 hours, 140  $\mu\text{L}$  of the supernatant was mixed with 10  $\mu\text{L}$  of 6.1 N trichloroacetic acid and the mixture was incubated for 30 min at 50 °C. The reaction mixture was then centrifuged for 10 minutes at 4000 rpm to remove sediments. 100  $\mu\text{L}$  of the supernatant was mixed with 100  $\mu\text{L}$  of 2% (w/v) *p*-dimethylaminobenzaldehyde in acetic acid and measured at 480 nm. The initial wells containing the cells in the remaining volume of 50  $\mu\text{L}$  were used to estimate cell viability in a classical MTT assay. To that end, 50  $\mu\text{L}$  of culture medium (Iscove medium with 10% FCS and amino acids) were added to the wells together with 20  $\mu\text{L}$  4 mg/mL of MTT. After 4 h of incubation at 37 °C, 200  $\mu\text{L}$  of DMSO were added to dissolve the crystals of formazan blue and the absorbance at 570 nm was measured after overnight incubation at 37 °C.

### 4.2.2. T-cell proliferation assay

T lymphocytes prepared from splenocytes of C57/bl6 mice were resuspended in RPMI 1640 containing 10% FBS, *L*-glutamate, penicillin, and streptomycin. The B16F1 cells were treated with mitomycin C at a final concentration of 25 mg/L and then incubated at 37 °C for 30 min. After being

washed three times, the B16F1 cells were resuspended in RPMI 1640 containing 10% FBS, L-glutamate, penicillin, and streptomycin.  $1 \times 10^5$  T lymphocytes (responder cells) and  $2 \times 10^4$  mitomycin C treated B16F1 cells (stimulator cells) were added to each well of a 96-well plate in RPMI 1640 containing 10% FBS in the presence of ConA (5  $\mu\text{g}/\text{mL}$ ). Cell proliferation was quantified by MTT assay. The cells were incubated at 37 °C and 5% CO<sub>2</sub> for 48 h; and 10  $\mu\text{L}$  MTT (4 mg/mL) was added to each well. MTT formazan production was dissolved by DMSO replacing the medium 4 h later. The absorbance at 570 nm (OD570) was measured by a microplate reader.

#### 4.2.3. Cytokine assays

Supernatant collected from the co-culture system were subjected to ELISA analysis for IFN- $\gamma$  by using kits from Dakawe (Beijing, China).

#### 4.2.4. Treg cells experiments

Treg cells were analyzed by using an eBioscience intracellular staining kit according to the manufacturer's instructions. After co-cultured with B16F1 cells, T cells were collected. Surface staining was performed with a CD4FITC and CD25PE for 15 min at 4 °C. After this, the cells were fixed and permeabilized with fixation buffer and permeabilization wash buffer. The intracellular staining was performed with FOXP3<sup>+</sup>APC for 20 min. The cells were then analyzed by flow cytometry analysis.

#### 4.2.5. Measurement of IDO1 absorbance spectra

Absorbance spectra (370-700 nm, Safire multifunction microplate reader) were measured immediately after addition of compounds (2 mM) to rhIDO1 (3  $\mu\text{M}$ ) in phosphate buffer (pH 6.5) using Safire multifunctional microplate reader. Ferrous form of the heme was obtained by adding sodium dithionite (10 mM) to the solution under N<sub>2</sub> atmosphere. Changes in the 424 nm maxima indicated binding to the ferrous iron of the heme.

### 4.3. Molecular modeling

#### 4.3.1. Average ESP analysis

Structural optimization of all compounds based on IFD calculation was conducted with the Lee–Yang–Parr correlation functional (B3LYP)/6-31G\*\* using Gaussian 09 software package [41]. Then, the wavefunction produced by QM calculation was employed for ESP analysis by Multiwfn [42]. ESP,

$V(r)$ , has been widely used for prediction of nucleophilic and electrophilic sites, as well as molecular recognition mode for a long time, the theoretical basis is that molecules always tend to approach each other in a complementary manner of ESP. These analyses of ESP are common performed on molecular van der Waals (vdW) surface. Through quantitative analysis of molecular surface, the average ESP on the local surface of the coordinating atom can be calculated to reveal characteristic of atom. It is well known that electrophiles always prefer to attack the atom which has very low ESP around it, so the coordinating atom with low ESP value should be an ideal reaction site for coordinate bond formation.

#### 4.3.2 *Induced fit docking*

In order to consider the flexibility of both ligand and protein, the *induced fit docking* protocol in Schrödinger was employed [43]. In IFD calculations, the ligands were first docked into the rigid receptor using softened energy function in *Glide*. By default, a maximum 20 poses per ligand were retained. Then, the protein degrees of freedom for each complex are sampled and the protein-ligand complexes were minimized. The protein structure in each pose now reflected an induced fit to the ligand structure and conformation. The best protein-ligand complex was then identified based on the predicted binding affinities of the docked ligand. Here, the residues within 5 Å of each of the 20 ligand poses were subjected to a conformational search and energy minimizations, and the residues outside this range were fixed. Finally, the minimized ligand was rigorously redocked into the induced-fit protein structure using *Glide XP* scoring mode, and metal constraints can be applied to both *Glide* docking stages in IFD protocol. The choice of the best-docked structure for each ligand was made using a model energy score that combines the energy grid score, the binding affinity predicted by GlideScore, and the internal strain energy for the model potential used to direct the conformational-search algorithm.

#### 4.3.3 *QM/MM geometry optimization.*

QM/MM calculations were performed via a two-layer *Qsite* program in Schrödinger [44]. *QSite* is a mixed mode QM/MM program used to study geometries and energies of structures not parameterized for use with molecular mechanics, such as those that contain metal. The reason for this may be complicated. For example, the partial charge of the metal cation is far from being at least approximately constant, and its value might be affected by many factors, for instance by switching the

oxidation state of the metal, the nature of the coordinated ligands, the solvation, and/or other environmental factors. Nevertheless, the MM simulation can be basically performed with a reasonable accuracy for a particular coordination sphere when only well-parametrized ligands of the metal interact with the complex surrounding. This is especially the case of a combined QM/MM method where the metal and its closest neighborhood are calculated at the QM level. *QSite* is uniquely equipped to perform QM/MM calculations because it combines the superior speed and power of *Jaguar* with the recognized accuracy of the OPLS force field. *Jaguar* is used for the quantum mechanical part of the calculations [45], and *Impact* provides the molecular mechanics simulation [46]. The QM region is the full heme ring, the Fe, the coordinating His residue and the inhibitor. This subsystem was optimized by employing density functional theory (DFT) using Becke's three-parameter hybrid exchange functional and B3LYP with the lacvp\* basis set and the convergence criterion for geometry optimizations followed the original *Qsite* defaults [47]. The remaining subsystem was treated with the MM method, and was geometry-optimized by using OPLS-2005 force field. The geometry optimization convergence criterion for MM subsystem was set as RMSD of energy gradient  $60 \text{ kcal mol}^{-1} \text{ \AA}^{-1}$ , and cutoff value was set to  $10 \text{ \AA}$  for non-bonded interactions during the QM/MM calculations. Throughout the QM/MM calculation, the cuts between the QM and MM regions were treated as specially parameterized frozen-orbital boundaries, which was placed between  $C_{\alpha}$  and  $C_{\beta}$  of the residue His346.

## Acknowledgments

Financial support from the National Natural Science Foundation of China (21472244, 21372261, 21472091 and 81673305) is gratefully acknowledge. This work was also supported by the Jiangsu Province Funds for Distinguished Young Scientists (BK20160033), the Six Major Talent Peak Project of Jiangsu Province (2011-YY-004), and the Fundamental Research Funds for the Central Universities (No. 2015021).

## References and notes

- [1] D.S. Vinay, E.P. Ryan, G. Pawelec, W.H. Talib, J. Stagg, E. Elkord, T. Lichtor, W.K. Decker, R.L. Whelan, H.M. Kumara, E. Signori, K. Honoki, A.G. Georgakilas, A. Amin, W.G. Helderich, C.S. Boosani, G. Guha, M.R. Ciriolo, S. Chen, S.I. Mohammed, A.S. Azmi, W.N. Keith, A. Bilsland, D. Bhakta, D. Halicka, H. Fujii, K. Aquilano, S.S. Ashraf, S. Nowsheen, X. Yang, B.K. Choi, B.S. Kwon,

- Immune evasion in cancer: Mechanistic basis and therapeutic strategies, *Semin. Cancer Biol.* 35 (2015) S185–S198.
- [2] D.H. Munn, A.L. Mellor, IDO in the tumor microenvironment: Inflammation, counter-regulation, and tolerance, *Trends Immunol.* 37 (2016) 193–207.
- [3] M. Platten, W. Wick, B.J. Van den Eynde, Tryptophan catabolism in cancer: beyond IDO and tryptophan depletion, *Cancer Res.* 21 (2012) 5435–5440.
- [4] I. Théate, N. van Baren, L. Pilotte, P. Moulin, P. Larrieu, J.C. Renaud, C. Hervé, I. Gutierrez-Roelens, E. Marbaix, C. Sempoux, B.J. Van den Eynde, Extensive profiling of the expression of the indoleamine 2,3-dioxygenase 1 protein in normal and tumoral human tissues, *Cancer Immunol. Res.* 2 (2015) 161–172.
- [5] U.M. Litzénbúrgér, C.A. Opitz, F. Sahm, K.J. Rauschenbach, S. Trump, M. Winter, M. Ott, K. Ochs, C. Lutz, X. Liu, N. Anastasov, I. Lehmann, T. Höfer, A. von Deimling, W. Wick, M. Platten, Constitutive IDO expression in human cancer is sustained by an autocrine signaling loop involving IL-6, STAT3 and the AHR, *Oncotarget* 5 (2014) 1038–1051.
- [6] M.W. Taylor, G.S. Feng, Relationship between interferon-gamma, indoleamine 2,3-dioxygenase, and tryptophan catabolism. *FASEB J.* 11 (1991) 2516–2522.
- [7] M.T. Pallotta, C. Orabona, C. Volpi, C. Vacca, M.L. Belladonna, R. Bianchi, G. Servillo, C. Brunacci, M. Calvitti, S. Bicciano, E.M. Mazza, L. Boon, F. Grassi, M.C. Fioretti, F. Fallarino, P. Puccetti, U. Grohmann. Indoleamine 2,3-dioxygenase is a signaling protein in long-term tolerance by dendritic cells, *Nat. Immunol.* 9 (2011) 870–878.
- [8] D.H. Munn, M.D. Sharma, B. Baban, H.P. Harding, Y. Zhang, D. Ron, A.L. Mellor, GCN2 kinase in T cells mediates proliferative arrest and anergy induction in response to indoleamine 2,3-dioxygenase, *Immunity* 22 (2005) 633–642.
- [9] R. Metz, S. Rust, J.B. Duhadaway, M.R. Mautino, D.H. Munn, N.N. Vahanian, C.J. Link, G.C. Prendergast, IDO inhibits a tryptophan sufficiency signal that stimulates mTOR: A novel IDO effector pathway targeted by *D*-1-methyl-tryptophan, *Oncoimmunology* 9 (2012) 1460–1468.
- [10] J.D. Mezrich, J.H. Fechner, X. Zhang, B.P. Johnson, W.J. Burlingham, C.A. Bradfield, An interaction between kynurenine and the aryl hydrocarbon receptor can generate regulatory T cells, *J. Immunol.* 185 (2010) 3190–3198.
- [11] N.T. Nguyen, A. Kimura, T. Nakahama, I. Chinen, K. Masuda, K. Nohara, Y. Fujii-Kuriyama, T. Kishimoto, Aryl hydrocarbon receptor negatively regulates dendritic cell immunogenicity via a kynurenine-dependent mechanism, *Proc. Natl. Acad. Sci. U. S. A.* 107 (2010) 19961–19966.
- [12] X. Liu, N. Shin, H.K. Koblish, G. Yang, Q. Wang, K. Wang, L. Leffet, M.J. Hansbury, B. Thomas, M. Rupa, P. Waeltz, K.J. Bowman, P. Polam, R.B. Sparks, E.W. Yue, Y. Li, R. Wynn, J.S. Fridman, T.C. Burn, A.P. Combs, R.C. Newton, P.A. Scherle, Selective inhibition of IDO1 effectively regulates mediators of antitumor immunity, *Blood* 17 (2010) 3520–3530.
- [13] C. Sheridan, IDO inhibitors move center stage in immuno-oncology, *Nat. Biotechnol.* 4 (2015)

321–322.

[14] S.G. Cady, M. Sono, 1-Methyl-*DL*-tryptophan, beta-(3-benzofuranyl)-*DL*-alanine (the oxygen analog of tryptophan), and beta-[3-benzo(*b*)thienyl]-*DL*-alanine (the sulfur analog of tryptophan) are competitive inhibitors for indoleamine 2,3-dioxygenase, *Arch. Biochem. Biophys.* 291 (1991) 326–333.

[15] D.Y. Hou, A.J. Muller, M.D. Sharma, J. DuHadaway, T. Banerjee, M. Johnson, A.L. Mellor, G.C. Prendergast, D.H. Munn, Inhibition of indoleamine 2,3-dioxygenase in dendritic cells by stereoisomers of 1-methyl-tryptophan correlates with antitumor responses, *Cancer Res.* 2 (2007) 792–801.

[16] A.J. Muller, J.B. DuHadaway, P.S. Donover, E. Sutanto-Ward, G.C. Prendergast, Inhibition of indoleamine 2,3-dioxygenase, an immunoregulatory target of the cancer suppression gene *Bin1*, potentiates cancer chemotherapy, *Nat. Med.* 11 (2005) 312–319.

[17] P. Vandenabeele, S. Grootjans, N. Callewaert, N. Takahashi, Necrostatin-1 blocks both RIPK1 and IDO: Consequences for the study of cell death in experimental disease models, *Cell Death Differ.* 20 (2013) 185–187.

[18] A. Degterev, J. Hitomi, M. Germscheid, I.L. Ch'en, O. Korkina, X. Teng, D. Abbott, G.D. Cuny, C. Yuan, G. Wagner, S.M. Hedrick, S.A. Gerber, A. Lugovskoy, J. Yuan, Identification of RIP1 kinase as a specific cellular target of necrostatins. *Nat. Chem. Biol.* 4 (2008) 313–321.

[19] P. Gaspari, T. Banerjee, W.P. Malachowski, A.J. Muller, G.C. Prendergast, J. DuHadaway, S. Bennett, A.M. Donovan, Structure-activity study of brassinin derivatives as indoleamine 2,3-dioxygenase inhibitors, *J. Med. Chem.* 2 (2006) 684–692.

[20] E. Dolušić, P. Larrieu, S. Blanc, F. Sapunarić, J. Pouyez, L. Moineaux, D. Colette, V. Stroobant, L. Pilotte, D. Colau, T. Ferain, G. Fraser, M. Galleni, J.M. Frere, B. Masereel, B. Van den Eynde, J. Wouters, R. Frédérick, Discovery and preliminary SARs of keto-indoles as novel indoleamine 2,3-dioxygenase (IDO) inhibitors, *Eur. J. Med. Chem.* 46 (2011) 3058–3065.

[21] E. Dolušić, P. Larrieu, S. Blanc, F. Sapunarić, B. Norberg, L. Moineaux, D. Colette, V. Stroobant, L. Pilotte, D. Colau, T. Ferain, G. Fraser, M. Galeni, J.M. Frere, B. Masereel, B. Van den Eynde, J. Wouters, R. Frédérick, Indol-2-yl ethanones as novel indoleamine 2,3-dioxygenase (IDO) inhibitors. *Bioorg. Med. Chem.* 19 (2011) 1550–1561.

[22] (a) S. Tojo, T. Kohno, T. Tanaka, S. Kamioka, Y. Ota, T. Ishii, K. Kamimoto, S. Asano, Y. Isobe, Crystal structures and structure-activity relationships of imidazothiazole derivatives as IDO1 inhibitors, *ACS Med. Chem. Lett.* 5 (2014) 1119–1123; (b) S. Qian, T. He, W. Wang, Y. He, M. Zhang, L. Yang, G. Li, Z. Wang, Discovery and preliminary structure-activity relationship of 1*H*-indazoles with promising indoleamine-2,3-dioxygenase 1 (IDO1) inhibition properties, *Bioorg. Med. Chem.* 24 (2016) 6194–6205; (c) W.P. Malachowski, M. Winters, J.B. DuHadaway, A. Lewis-Ballester, S. Badir, J. Wai, M. Rahman, E. Sheikh, J.M. LaLonde, S.R. Yeh, G.C. Prendergast, A.J. Muller, *O*-alkylhydroxylamines as rationally-designed mechanism-based inhibitors of indoleamine 2,3-dioxygenase-1, *Eur. J. Med. Chem.* 108 (2016) 564–576.

- [23] (a) U.F. Rohrig, S.R. Majjigapu, M. Chambon, S. Bron, L. Pilotte, D. Colau, B.J. Van den Eynde, G. Turcatti, P. Vogel, V. Zoete, O. Michielin, Detailed analysis and follow-up studies of a high-throughput screening for indoleamine 2,3-dioxygenase 1 (IDO1) inhibitors, *Eur. J. Med. Chem.* 84 (2014) 284–301; (b) M.F. Cheng, M.S. Hung, J.S. Song, S.Y. Lin, F.Y. Liao, M.H. Wu, W. Hsiao, C.L. Hsieh, J.S. Wu, Y.S. Chao, C. Shih, S.Y. Wu, S.H. Ueng, Discovery and structure-activity relationships of phenyl benzenesulfonylhydrazides as novel indoleamine 2,3-dioxygenase inhibitors, *Bioorg. Med. Chem. Lett.* 24 (2014) 3403–3406; (c) J.A. Markwalder, S.P. Seitz, Y. Blat, L. Elkin, J.T. Hunt, J.G. Pabalan, M.N. Jure-Kunkel, G.D. Vite, K. Covello, Identification and optimization of a novel series of indoleamine 2,3-dioxygenase inhibitors, *Bioorg. Med. Chem. Lett.* 27 (2017) 582–585.
- [24] (a) M. Tanaka, X. Li, H. Hikawa, T. Suzuki, K. Tsutsumi, M. Sato, O. Takikawa, H. Suzuki, Y. Yokoyama, Synthesis and biological evaluation of novel tryptoline derivatives as indoleamine 2,3-dioxygenase (IDO) inhibitors, *Bioorg. Med. Chem.* 21 (2013) 1159–1165; (b) R. Pasceri, D. Siegel, D. Ross, C.J. Moody, Aminophenoxazinones as inhibitors of indoleamine 2,3-dioxygenase (IDO). Synthesis of exfoliazone and chandrananimycin A, *J. Med. Chem.* 56 (2013) 3310–3317; (c) S. Yang, X. Li, F. Hu, Y. Li, Y. Yang, J. Yan, C. Kuang, Q. Yang, Discovery of tryptanthrin derivatives as potent inhibitors of indoleamine 2,3-dioxygenase with therapeutic activity in Lewis lung cancer (LLC) tumor-bearing mice, *J. Med. Chem.* 56 (2013) 8321–8331; (d) R.M. Centko, A. Steino, F.I. Rosell, B.O. Patrick, N. de Voogd, A.G. Mauk, R.J. Andersen, Indoleamine 2,3-dioxygenase inhibitors isolated from the Sponge *Xestospongia vansoesti*: Structure elucidation, analogue synthesis, and biological activity, *Org. Lett.* 16 (2014) 6480–6483; (e) E. Dolusic, P. Larrieu, C. Meinguet, D. Colette, A. Rives, S. Blanc, T. Ferain, L. Pilotte, V. Stroobant, J. Wouters, B. Van den Eynde, B. Masereel, E. Delfourne, R. Frederick, Indoleamine 2,3-dioxygenase inhibitory activity of derivatives of marine alkaloid tsitsikammamine A, *Bioorg. Med. Chem. Lett.* 23 (2013) 47–54.
- [25] E. Vacchelli, F. Aranda, A. Eggermont, C. Sautes-Fridman, E. Tartour, E.P. Kennedy, M. Platten, L. Zitvogel, G. Kroemer, L. Galluzzi, Trial watch: IDO inhibitors in cancer therapy, *OncoImmunology*, 3 (2014) e957994.
- [26] <https://www.clinicaltrials.gov/ct2/results?term=IDO&Search=Search>.
- [27] L. Capece, M. Arrar, A.E. Roitberg, S.R. Yeh, M.A. Marti, D.A. Estrin, Substrate stereo-specificity in tryptophan dioxygenase and indoleamine 2,3-dioxygenase, *Proteins* 78 (2010) 2961–2972.
- [28] S. Kumar, D. Jaller, B. Patel, J.M. LaLonde, J.B. DuHadaway, W.P. Malachowski, G.C. Prendergast, A.J. Muller, Structure based development of phenylimidazole-derived inhibitors of indoleamine 2,3-dioxygenase, *J. Med. Chem.* 51 (2008) 4968–4977.
- [29] E.W. Yue, B. Douty, B. Wayland, M. Bower, X. Liu, L. Leffet, Q. Wang, K.J. Bowman, M.J. Hansbury, C. Liu, M. Wei, Y. Li, R. Wynn, T.C. Burn, H.K. Koblish, J.S. Fridman, B. Metcalf, P.A. Scherle, A.P. Combs, Discovery of potent competitive inhibitors of indoleamine 2,3-dioxygenase with in vivo pharmacodynamic activity and efficacy in a mouse melanoma model, *J. Med. Chem.* 52 (2009)

7364–7367.

[30] C. Uyttenhove, L. Pilotte, I. Theate, V. Stroobant, D. Colau, N. Parmentier, T. Boon, B.J. Van den Eynde, Evidence for a tumoral immune resistance mechanism based on tryptophan degradation by indoleamine 2,3-dioxygenase, *Nat. Med.* 9 (2003) 1269–1274.

[31] D.H. Munn, Blocking IDO activity to enhance anti-tumor immunity, *Front. Biosci.* 4 (2012) 734–745.

[32] S. Panda, A. Roy, S.J. Deka, V. Trivedi, D. Manna, Fused heterocyclic compounds as potent indoleamine-2,3-dioxygenase 1 inhibitors, *ACS Med. Chem. Lett.* 7 (2016) 1167–1172.

[33] Y.H. Peng, S.H. Ueng, C.T. Tseng, M.S. Hung, J.S. Song, J.S. Wu, F.Y. Liao, Y.S. Fan, M.H. Wu, W.C. Hsiao, C.C. Hsueh, S.Y. Lin, C.Y. Cheng, C.H. Tu, L.C. Lee, M.F. Cheng, K.S. Shia, C. Shih, S.Y. Wu, Important hydrogen bond networks in indoleamine 2,3-dioxygenase 1 (IDO1) inhibitor design revealed by crystal structures of imidazoleisoindole derivatives with IDO1, *J. Med. Chem.* 59 (2015) 282–293.

[34] F. Šebesta, V. Sláma, J. Melcr, Z. Futera, J.V. Burda, Estimation of transition-metal empirical parameters for molecular mechanical force fields, *J. Chem. Theory Comput.* 12 (2016) 3681–3688.

[35] U.F. Rohrig, S.R. Majjigapu, P. Vogel, V. Zoete, O. Michielin, Challenges in the discovery of indoleamine 2,3-dioxygenase 1 (IDO1) inhibitors, *J. Med. Chem.* 58 (2015) 9421–9437.

[36] A. Bach, D. Pizzirani, N. Realini, V. Vozella, D. Russo, I. Penna, L. Melzig, R. Scarpelli, D. Piomelli, Benzoxazolone carboxamides as potent acid ceramidase inhibitors: Synthesis and structure–activity relationship (SAR) studies, *J. Med. Chem.* 58 (2015) 9258–9272.

[ 37 ] W. Dölling, K. Kischkies, F. Heinemann, H. Hartung, Synthesis of alkyl 2-(2-oxo-benzazoline-3-yl)-3-hydroxy  $\alpha,\beta$ -unsaturated dithiocarboxylates and the corresponding ketene dithioacetals. Their crystal and molecular structures, *Monatsh. Chem.* 124 (1993) 707–719.

[ 38 ] S. Dalkara, U. Calis, R. Sunal, Synthesis and anticonvulsant activity of some new 2(3*H*)-benzoxazolone derivatives, *J. Pharm. Belg.* 43 (1988) 372–378.

[39] D.S. Goldfarb, Method for altering the lifespan of eukaryotic organisms, 2009. U.S. Pat. Appl. US 20090163545.

[40] D. Piomelli, C. Pagliuca, D. Pizzirani, A. Bach, N. Realini, M. DeVivo, Preparation of benzoxazolone derivatives as acid ceramidase inhibitors, and their use as medicaments, 2015. PCT Int. Appl. WO2015173168.

[41] Gaussian 09, Revision D.01, M.J. Frisch, G.W. Trucks, H.B. Schlegel, G.E. Scuseria, M.A. Robb, J.R. Cheeseman, G. Scalmani, V. Barone, B. Mennucci, G.A. Petersson, H. Nakatsuji, M. Caricato, X. Li, H.P. Hratchian, A.F. Izmaylov, J. Bloino, G. Zheng, J.L. Sonnenberg, M. Hada, M. Ehara, K. Toyota, R. Fukuda, J. Hasegawa, M. Ishida, T. Nakajima, Y. Honda, O. Kitao, H. Nakai, T. Vreven, J.A. Montgomery Jr., J.E. Peralta, F. Ogliaro, M. Bearpark, J.J. Heyd, E. Brothers, K.N. Kudin, V.N. Staroverov, T. Keith, R. Kobayashi, J. Normand, K. Raghavachari, A. Rendell, J.C. Burant, S.S. Iyengar, J. Tomasi, M. Cossi, N. Rega, J.M. Millam, M. Klene, J.E. Knox, J.B. Cross, V. Bakken, C.

Adamo, J. Jaramillo, R. Gomperts, R.E. Stratmann, O. Yazyev, A.J. Austin, R. Cammi, C. Pomelli, J.W. Ochterski, R.L. Martin, K. Morokuma, V.G. Zakrzewski, G.A. Voth, P. Salvador, J.J. Dannenberg, S. Dapprich, A.D. Daniels, O. Farkas, J.B. Foresman, J.V. Ortiz, J. Cioslowski, D.J. Fox, Gaussian, Inc., Wallingford CT, 2013.

[42] T. Lu, F. Chen, Multiwfn: a multifunctional wavefunction analyzer, *J. Comp. Chem.* 33 (2012) 580–592.

[43] Induced Fit Docking protocol, Glide version 5.5, Prime version 2.1, Schrödinger, LLC, New York, NY, 2009.

[44] QSite, version 5.1, Schrödinger, LLC, New York, NY, 2009.

[45] Jaguar, version 7.6, Schrödinger, LLC, New York, NY, 2009.

[46] Impact, version 5.5, Schrödinger, LLC, New York, NY, 2009.

[47] P.J. Hay, W.R. Wadt, Ab initio effective core potentials for molecular calculations. Potentials for K to Au including the outermost core orbitals, *J. Chem. Phys.* 82 (1985) 299–310.

**Highlights:**

- A scaffold-hopping strategy combined with the average electrostatic potentials calculation was utilized to design novel benzoxazolinone derivatives.
- A novel interesting scaffold for IDO1 inhibition was identified.
- T-cell proliferation and Tregs assays were performed to evaluate the capacity of the compounds in the reversal of IDO1-mediated immunosuppression.
- UV spectroscopic experiment provided a direct evidence of our compounds binding to the active site of IDO1.
- The induced fit docking and QM/MM calculation were performed to predict the binding mode of IDO1 and its ligand.